NTNU – Trondheim
Norwegian University of
Science and Technology

Optimization in CT

Evaluation of dose saving potential in a thorax-abdomen/pelvis protocol using iterative reconstruction techniques

Ingvild Dalehaug

Master of Science in Physics and Mathematics
Submission date: June 2013
Supervisor: Tore Lindmo, IFY
Co-supervisor: Kirsten Bolstad, Haukeland universitetssjukehus

Norwegian University of Science and Technology
Department of Physics

DIPLOMA THESIS

Optimization in CT

Evaluation of dose saving potential in a thorax-abdomen/pelvis protocol using iterative reconstruction techniques

Ingvild Dalehaug

Spring 2013

Norwegian University of Science and Technology – NTNU
Faculty of Natural Sciences and Technology
Department of Physics

PREFACE AND ACKNOWLEDGEMENTS

This thesis completes my Master's Degree in Biophysics and Medical Technology at the Department of Physics, Faculty of Natural Science and Technology at the Norwegian University of Science and Technology, NTNU, Trondheim. The study was performed at the Medical Physics Section, Department of Oncology and Medical Physics at Haukeland University Hospital during the spring 2013.

First of all, I would like to thank my great supervisor medical physicist Kirsten Nygaard Bolstad for the excellent follow-up during these six months. The regularly comprehensive feedback during the writing of this thesis has been highly appreciated.

In addition a physicist Helge Pettersen deserves a special thank for helping me by making valuable programs in Python, in addition to great feedback on my written work and very helpful discussions.

I will also express my thanks to Tore Lindmo, my external supervisor at NTNU, for thorough feedback on my thesis prior to submission, it was very helpful.

I am also grateful for the valuable feedback from physicist Kristine Fasmer on the theory the PSF_Noise and great guidance in using the program.

In the end a great thank to the head of the department, Anfinn Mehus for giving me the great opportunity of writing the thesis here and radiologists Lars Reisæter and Gaute Wathle for taking the time to evaluate some of my CT scans.

Bergen, June 15th, 2013

Ingvild Dalehaug

ABSTRACT

The use of computed tomography (CT) has increased dramatically during the last two decades and contributes today to 80% of the estimated population dose caused by radiological examinations. Recent publications have shown an increased incidence of cancer caused by the irradiation from CT examinations and has led to increased dose awareness.

In this study the dose saving potential for a thorax-abdomen/pelvis protocol on a Siemens SOMATOM Definition AS + (Siemens, Germany) was investigated. The main aim was to reduce the dose to the patient while maintaining similar image quality as the current scan protocol. Alternative reconstruction filters and using iterative techniques where applied to lower dose scans of a Catphan 600 phantom (Siemens Germany). Physical and objective image quality parameters, in this case the spatial resolution, noise and noise power spectrum (NPS) curves were measured in the lower dose scans of Catphan 600 and compared to the spatial resolution, noise and NPS measured in the current scan protocol. The parameter settings resulting in similar objective image quality where applied to scans of an anthropomorphic phantom. Signal to noise ratio (SNR) and contrast to noise ratio (CNR) where calculated and compared to SNR and CNR of the current scan protocol. The final best lower dose alternatives where presented for experienced radiologists for subjective evaluation.

Physical image quality parameters such as spatial resolution, noise level, SNR and CNR were found to be maintained down at 50% dose level. However, the NPS curves revealed some minor shift in spatial distribution of the noise towards coarser graininess at the highest iterative strengths. The experienced thorax radiologist qualified all lower dose alternatives presented as diagnostically acceptable. The experienced gastro radiologist evaluated the scans reconstructed with a higher iterative level than 2 as blotchy and not diagnostically suitable. The observed blotchiness may have a correlation with the minor shift in NPS curves.

In conclusion, a dose level of 75% (i.e. 25% lower dose than the current scan protocol) using higher iterative strength was found to be diagnostically acceptable and can be further explored on patients.

ABBREVIATIONS AND SYMBOLS

- CNR: Contrast to Noise Ratio
- CT: Computed Tomography
- Gy: Grey
- HU: Hounsfield Unit
- LSF: Line Spread Function
- mSv: miliSievert
- MTF: Modulating Transfer Function
- NPS: Noise Power Spectrum
- PSF: Point Spread Function
- SAFIRE: Sinogram Affirmed Iterative Reconstruction
- $\boldsymbol{\sigma}_{\mathrm{HU}}$: standard deviation of the pixel values, given in Hounsfield Units (=Noise)
- SNR: Signal to Noise Ratio
- STD: Standard Deviation

TABLE OF CONTENT

1 INTRODUCTION

Today, approximately 900 radiological examinations per 1000 inhabitants are performed each year in Norway. The estimated population dose resulting from radiological examinations is 1.1 mSv per person per year, where computed tomography, CT, contributes to 80% of this dose. From 2002 to 2008 the number of CT scans performed in Norway doubled (NRPA 2010). Some reasons for this increased use of CT-scans might be the use of CT in the follow-up of cancer patients, the use of CT at the emergency rooms to get an overview of the injuries, and an increasing use of CT on symptom free patients requesting examinations themselves (NRPA 2010; Bakke 2011). Organ doses from CT scans are often a factor of 10 times higher than from conventional X-ray examinations. Organ dose for a set of CT scans may range from 5 mSv to 100 mSv, depending on factors like number of scans, type of scans, machine setting and age/size variability. In this dose range, there is epidemiological evidence of a small, but statistically significant increase in cancer risk based on the statistics from the atomic bomb survivors from Hiroshima (Brenner 2010).

With these numbers in hand, it is not difficult to understand the importance of reducing doses to patients while maintaining good enough image quality when performing a CT examination.

The harmful effects of ionizing radiation fall mainly into two categories: Stochastic effects and deterministic effects. Deterministic effects are effects that occur above a certain threshold dose, with increasing severity when first crossing the threshold value. Stochastic effects don't have any threshold dose value, but the probability of occurring increases with increasing dose. If the stochastic effects first occur, the severity is independent of the received dose. Examples of deterministic effects is eye cataract with threshold doses at 0,5 Gy (Hall and Giaccia 2012). An example of stochastic effect is radiation induced cancer, where the effect may occur 20-30 years after radiation exposure (Hall and Giaccia 2012). The stochastic effects are of importance, since they don't have any lower threshold dose that can be considered safe. Due to this, all X-ray

examinations should be performed with precaution, after the ALARA principle, an acronym for As Low As Reasonable Achievable, which states that the dose to the patient should be as low as it can be without losing relevant diagnostic information.

1.1 MOTIVATION

In this study, the optimization potential on a thorax – abdomen/pelvic examination has been examined. This examination covers a large volume of the patient containing several vital and radiation-sensitive organs (Hall and Giaccia 2012). Generally reduced patient dose, while maintaining an acceptable image quality for this specific protocol may have a significant impact on this patient group at Haukeland University Hospital as most of these patients are cancer patients coming in for cancer follow-up every third month. There was a request from the management at the radiological department on optimizing this particular procedure as many patients undergo this examination.

The noise increase at lower doses and low-contrast object detection is reduced with increasing noise (Curry, Dowdey et al. 1990) In the abdomen area the most significant challenge related to lowering the dose is the loss of low-contrast object detectability. Different diseases, for instance metastasis in any of the parenchymal organs (liver, pancreas, gallbladder, spleen and biliary ducts) or neoplastic disease, manifest as a low-attenuation objects within a background of slightly higher attenuation (Baker, Dong et al. 2012).. It is therefore critical that the level of noise remains the same as it is for todays' protocol when optimizing this protocol (Baker, Dong et al. 2012).

In the thorax area, there is a high inherent contrast between lung tissue and air (Yang, Yan et al. 2013). The low attenuation in the lung area generates much less noise than the abdomen area. However, due to dose modulation (see chapter 2.2.2) the dose given in this area is much lower, generating similar noise level as in the abdomen area.

The main goal of this study was to investigate the image quality for a thorax-abdomen-pelvis protocol on a Siemens SOMATOM Definition AS+ CT-scanner when examining dose levels of 50%, 62,5% and 75% compared to the current dose level. The aim was to keep the measured objective image quality at the same level as today's protocol by adding iterative reconstruction and exploring alternative filters.

2 THEORY

2.1 RADIATION DOSE IN CT

During a CT scan, the exposure is continuous around the patient in contrast to traditional X-ray where the exposure is at its maximum at the entrance (See Figure 1).

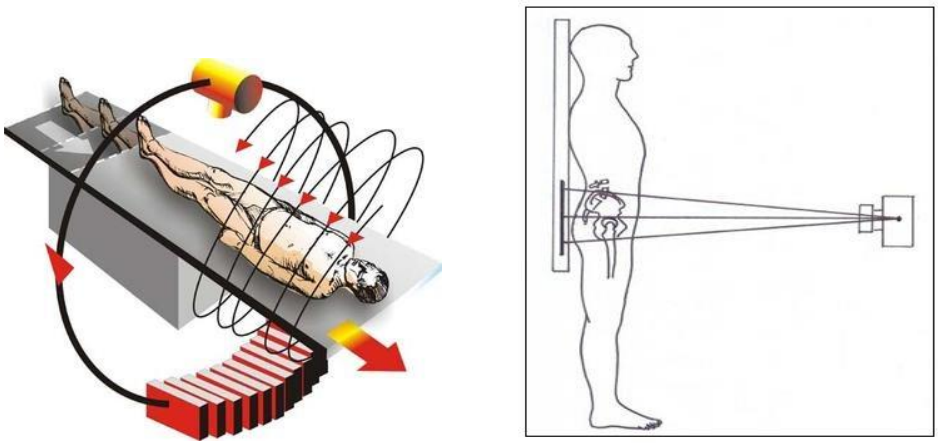

Figure 1: A sketch of a helical CT scan. The patient table move forward in the often referred to as the z-direction, while the X-ray tube with detectors on the opposite site moves around the patient in a helical manner. The sketch to the left illustrates the traditional projection X-ray.(www.radiologie-idar-oberstein.com 2013)

The CT typically uses thin slices (0.5 mm- 20 mm thickness) taken along the z-axis to be able to visualize an entire body part. In conventional X-ray the projection radiographic exposure is taken from one source position, making the entrance skin dose much larger than the exit skin dose. In contrast, the helical exposure from CT scans with a full 360 degrees rotation results in a radially symmetric radiation dose (See Figure 2).

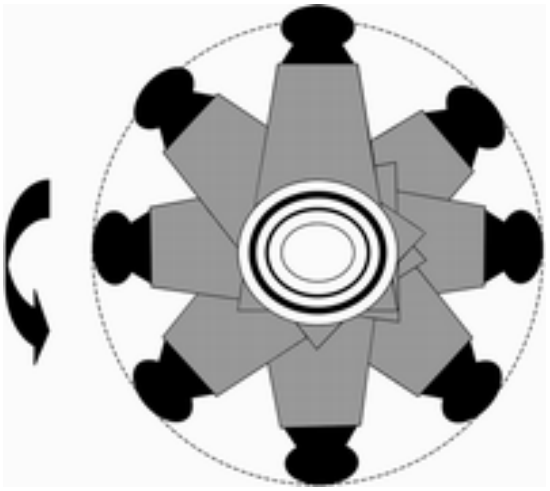

Figure 2: Dose gradient from a full 360° exposure from a CT scan. The thicker circles represent entrance skin dose which is much larger than the dose at the inner radius. However, the dose is radially symmetric (McNitt-Gray 2002).

2.1.1 SOME FACTORS DIRECTLY INFLUENCING RADIATION DOSE FROM CT

Photon fluence

The tube current time product, mAs, is directly proportional to the photon fluence, which is again proportional to the dose given to the patient.

Helical pitch

The pitch parameter, defined as the distance traveled along the z-axis of the table during one 360° rotation, has a direct influence on patient radiation dose.

$$p = \frac{T}{b}$$

Equation 1: p is pitch parameter, T is table increment during one 360° rotation and b is nominal slice thickness as visualized by the thickness of the greens strips in Figure 3. (Webb and Flower 2012)

When the pitch increases while keeping all other scan parameters constant, the exposure at any given point is decreased as the X-ray beam moves faster on to the next point, see Figure 3. With a pitch of 1 there is no space between the nominal slices, a pitch <1 gives overlapping, while a pitch>1 gives space between the nominal slices.

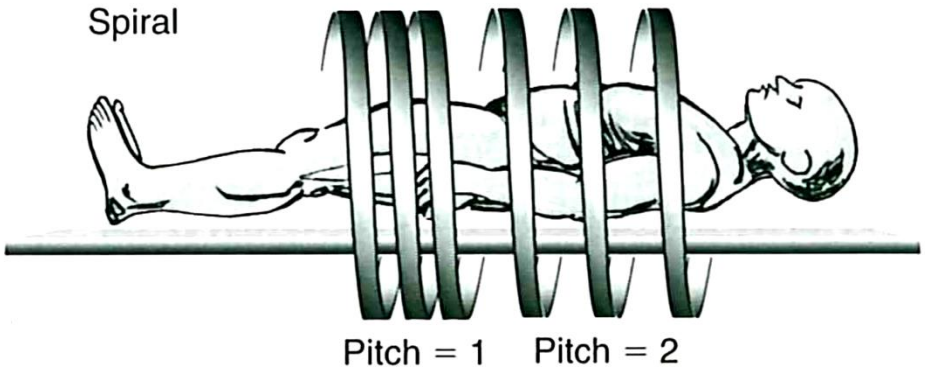

Figure 3: The figure illustrates the concept of pitch.

Patient size

A larger patient will attenuate a larger part of the X-ray beam, making a higher dose necessary.

2.1.2 POSSIBLE WAYS OF REDUCING RADIATION DOSE

There are several ways of reducing the dose per CT scan. Reducing the mAs value, or increasing the pitch will all reduce the dose to the patient. However, these reductions will also give significant reduction in image quality (McNitt-Gray 2002). Nevertheless, different diagnostic tasks require different image quality, giving possibilities to allow poorer image quality in some cases. Dose versus image quality should always follow the ALARA principle (As Low As Reasonable Achievable) (RSNA.org 2013).

An indirect way of reducing the radiation dose is by using reconstruction techniques to improve the image quality by reducing the noise, thereby generating a potential for reducing dose without sacrificing the image quality (Baumueller, Winklehner et al. 2012; Fletcher, Grant et al. 2012; Martinsen, Saether et al. 2012).

2.2 PRINCIPLES OF COMPUTED TOMOGRAPHY (CT)

X-ray computed tomography aim to give a 3D-representation of the internal structures of an object by irradiating the object from many different angles (Ghetti, Ortenzia et al. 2012; Webb and Flower 2012). When a planar slice of the object is irradiated by X-rays, a projection profile, which reflects the X-ray beam intensity reaching the detector for the specific angle, can be obtained. See Figure 4. (Webb and Flower 2012)

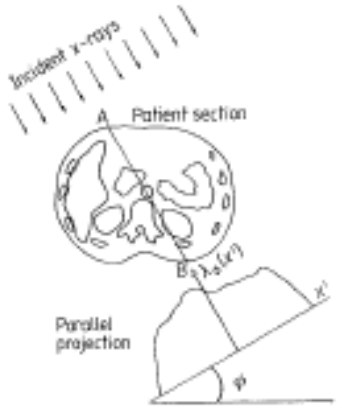

Figure 4: The figure illustrates the projection profile obtained when irradiating the patient from angle ϕ (Webb 1988; Webb and Flower 2012) .

A single projection $\lambda_\phi(x')$, outlined as AB in Figure 4 can mathematically be described as

$$\lambda_{\boldsymbol{\phi}}(x') = -\ln \frac{I_\phi(x')}{I_{\phi 0}(x')}$$

$$= \iint_{-\infty}^{\infty} \mu[x, y]\delta(x\,cos\phi + y\,sin\phi - x')dxdy$$

$I_{\phi 0}(x')$ and $I_{\phi}(x')$ is the unattenuated and attenuated intensity, respectively. $\mu[x, y]$ is the two dimensional distribution of the linear attenuation coefficients, while $\boldsymbol{\phi}$ and x' define the position of the measurement. The Dirac's Delta function δ picks out the path of the line integral.

By utilizing the information on the projection profiles from all angles, it is possible to reconstruct the attenuation coefficients $\mu[x, y]$ from the projections $\lambda_{\phi}(x')$.

This planar slice has a certain thickness and together with the matrix size (see Figure 5) this is what constitutes what is called a voxel (See Figure 5). From one voxel only a single attenuation coefficient can be obtained. This attenuation coefficient is rescaled to a CT number before being displayed on a monitor, defined as

$$CT\ number = \frac{(\mu_{tissue} - \mu_{water})}{\mu_{water}} \cdot 100$$

and given in terms of Hounsfield units (HU). The CT number gives the fractional difference of its linear attenuation coefficient relative to water. An image slice of a CT scan gives an attenuation coefficient map, where tissue of same material will have the same CT numbers at a given kV.

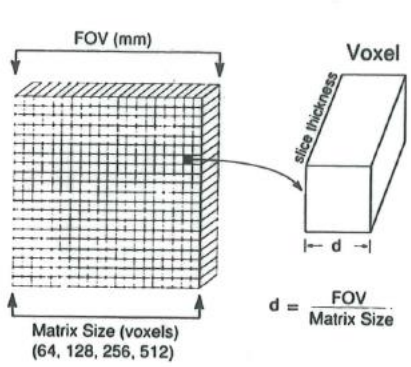

Figure 5: The figure illustrates the correlation between field of view (which is set by the user), slice thickness and matrix size (Sprawls 1992).

2.2.1 HELICAL CT

The CT scanners have gone through major developments since they first entered the marked in 1973 (Webb and Flower 2012).The planar slice geometry where the X-ray tube makes a full rotation before the patient table is shifted and a new 360 degree turn is taken, has been exchanged with helical CT, where the X-ray tube and the detector continuously rotates while the patient table moves forward in the z-direction (see Figure 6).

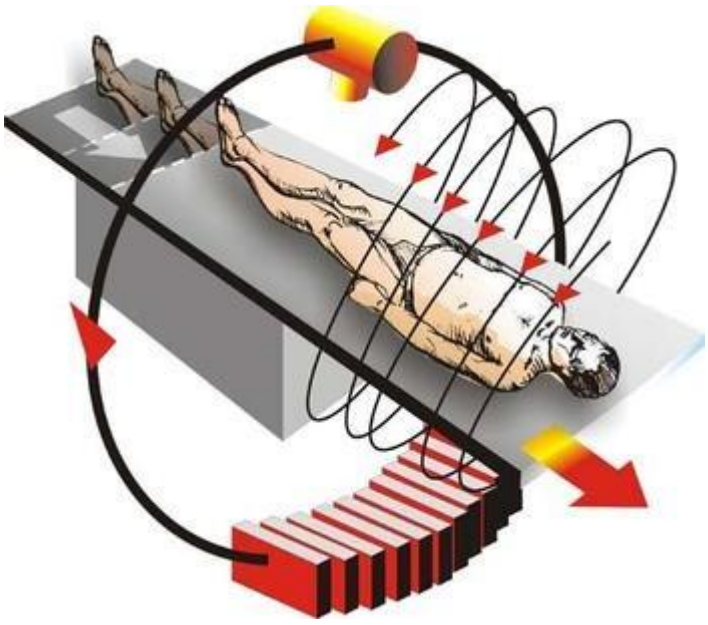

Figure 6: The figure gives an illustration of helical CT. The X-ray tube and the detectors rotates steadily 360 degrees, while the patient table moves forward, generating a helical path (www.radiologie-idar-oberstein.com 2013).

Due to the helical path formed by the rotating X-ray tube and detector and the moving table, only a few projections are available in a given reconstruction plane perpendicular to the direction of motion. Before image reconstruction can take place, a full set of projections must be obtained at a specific slice location. This is done by interpolation, where the missing projections are estimated by taking the average between the two closest projections available at the desired projection angle (Webb and Flower 2012).

2.2.2 AUTOMATIC EXPOSURE CONTROL

Today, all vendors have their version of automatic exposure control. When keeping the exposure value constant over the entire scan, the image noise will be lower in regions with lower attenuation as more photons reach the detector (see 2.4.2 on noise). To obtain similar image noise over the whole scan, the exposure value can be reduced in areas with lower attenuation such as the thorax area, and increased in areas with higher attenuation such as the pelvic area. This is the essential principle behind dose modulation. More precisely, the tube current is adapted along the scanning direction (z-axis) based on an attenuation profile obtained from a topogram (a CT projection radiograph, see Figure 7) prior to the examination. By using a "sophisticated algorithm" the attenuation profile perpendicular to the projection direction is also calculated (Siemens 2013).

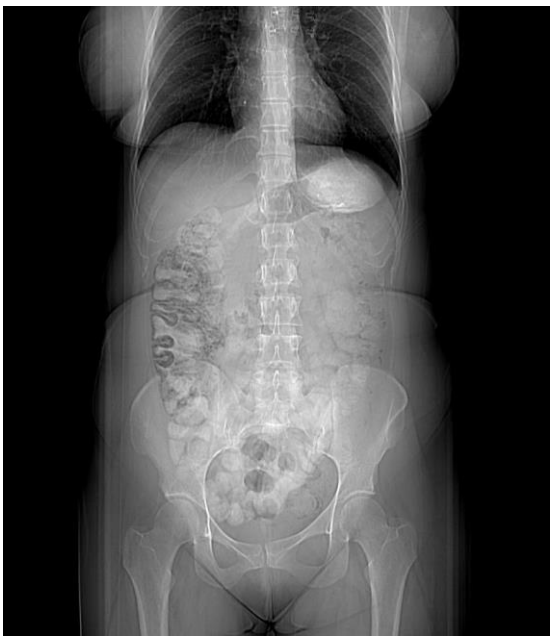

Figure 7: Example of a topogram taken prior to a CT examination (Department of Radiology 2013).

As a patient does not have a perfect circular shape, the amount of tissue the X-ray beam traverses as the detectors rotates around the patient is strongly dependent on the angle. For instance, when the X-ray beam is positioned posterior to the patient in the shoulder region, the beam will be less attenuated than when positioned in the lateral direction (See Figure 8). Due to this, the tube current is also adapted in real time in the angular direction as visualized by the blue graph in figure 15.

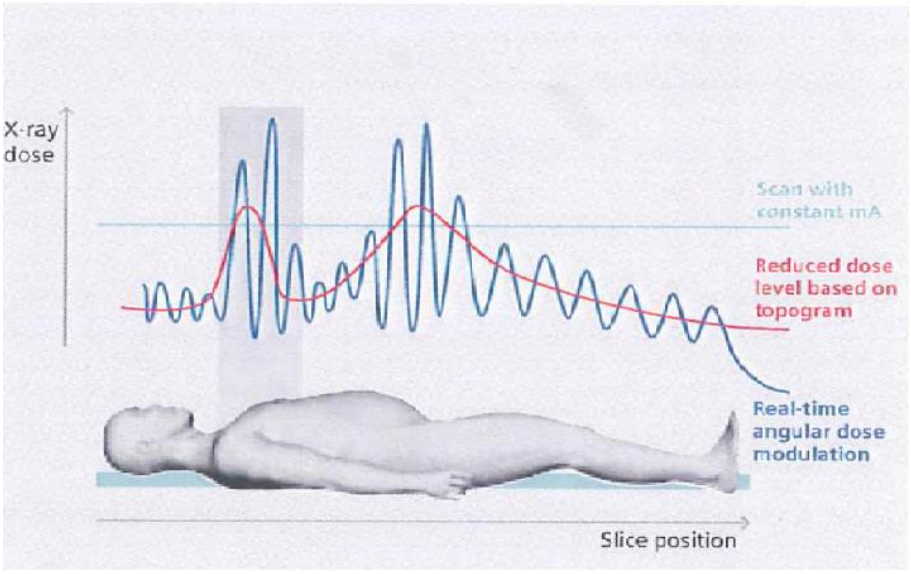

Figure 8: The red graph shows how the dose varies as a function of position along the z-axis. The blue graph shows the angular variation. (Siemens 2013)

In addition, when adjusting for obese patients, a higher level of noise can be accepted, as larger patients also provide greater contrast due to inter-abdominal fat. In the opposite case, when examining slim patients, a smaller noise level must be set, as the contrast is poorer.

When using Siemens dose modulation, CAREDose4D, the user sets a so called "image quality reference mAs", which for a given protocol reflects the effective mAs needed to gain this image quality for a "typical adult," weighing 70 kg to 80 kg.

From the topogram the dose modulating software determines whether the patient can be considered normal, slim or obese and thereafter adjust the tube current after the preselected adaption strength (See Figure 9). For a small patient, the tube current is reduced less than constant image noise would require, while for an obese patient the tube current is increased less than constant image noise would require (See Figure 9).

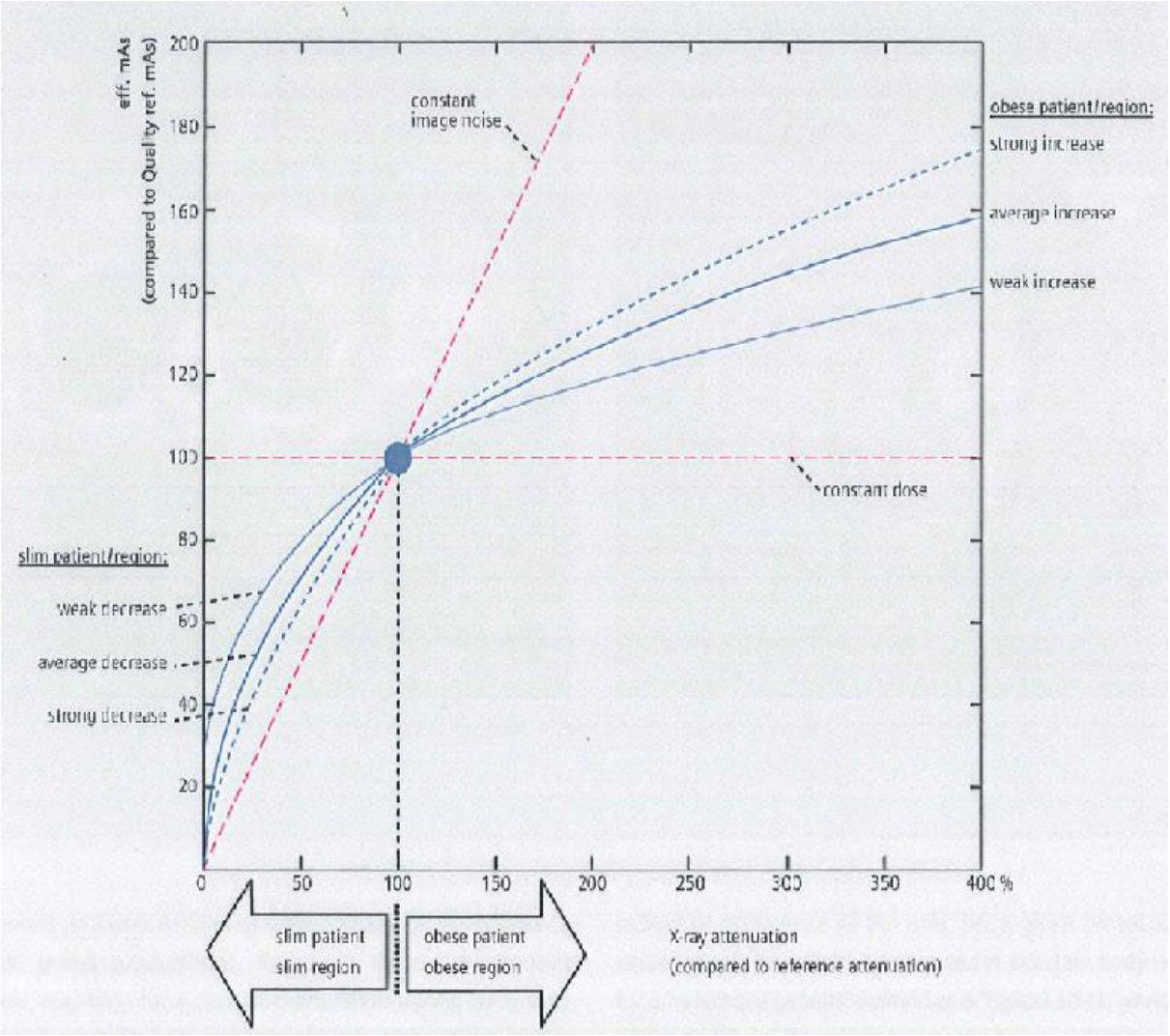

Figure 9: How much the tube current will adapt the patient size can be chosen by the user (Siemens 2013).

2.3 RECONSTRUCTION ALGORITHMS

There are mainly two different reconstruction algorithms used today to obtain an image based on the information from the projection profiles, filtered back projection (FBP) and iterative reconstruction. However, recently, also model-based methods have entered the marked, which try to model the acquisition process as accurate as possible (Beister, Kolditz et al. 2012) to be able to calculate and remove the noise from the image.

2.3.1 FILTERED BACK PROJECTION

The concept of back projection is illustrated in Figure 10. The projection profiles obtained for each radiation angle are superimposed to produce a crude reproduction of the original image. All points in the back-projected image receive density contributions from neighboring structures, which will result in a blurry image, even when using a

great number of projections. To reduce this blurriness, the projection data is filtered prior to reconstruction to counterbalance the effect of the sudden density changes (Curry, Dowdey et al. 1990). See Figure 11.

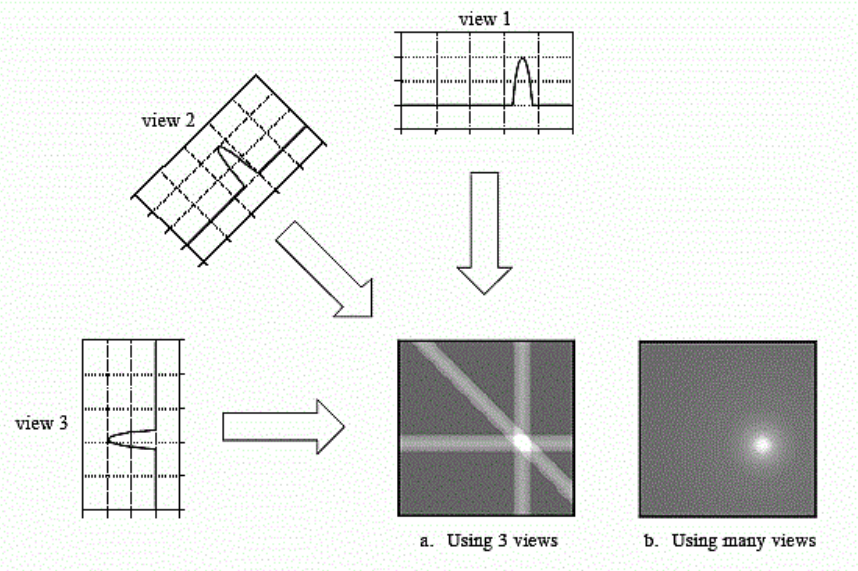

Figure 10: Back projection of the projection profiles reconstructs an image by taking each view and smearing it along the path it was originally acquired. The resulting image is a blurry image of the object (Smith 2002).

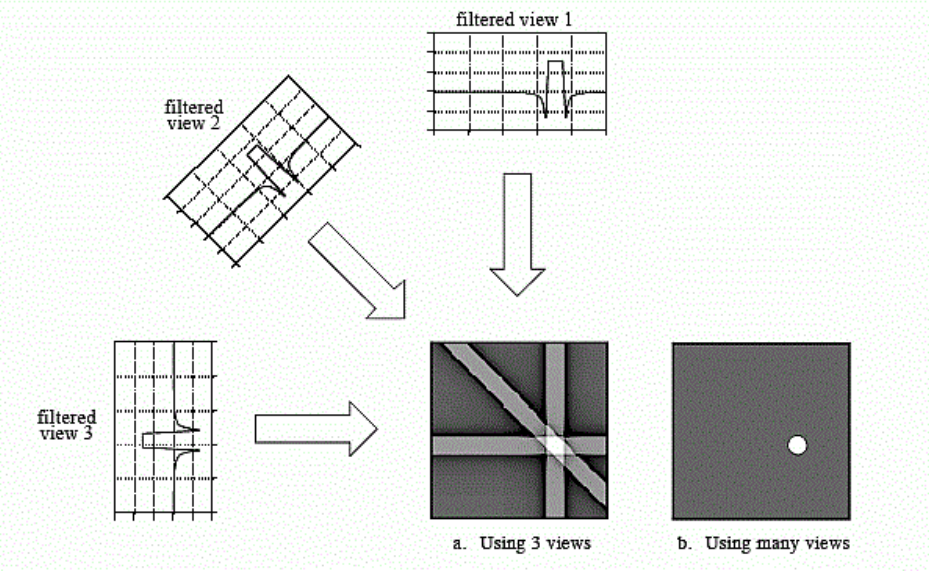

Figure 11: Filtered back projection reconstructs an image by filtering each view before back projecting it. This removes the blurring seen in simple back projection (Smith 2002).

The user can select from a variety of different reconstruction filters (see Table 1). A sharp filter (see Figure 12) will emphasize high spatial frequencies giving rise to sharper

edges. However, a sharp filter will also emphasize the high frequent noise, giving rise to a noisier image (see Figure 13, the image to the right). To suppress noise a smooth filter can be applied (Figure 13 to the left).

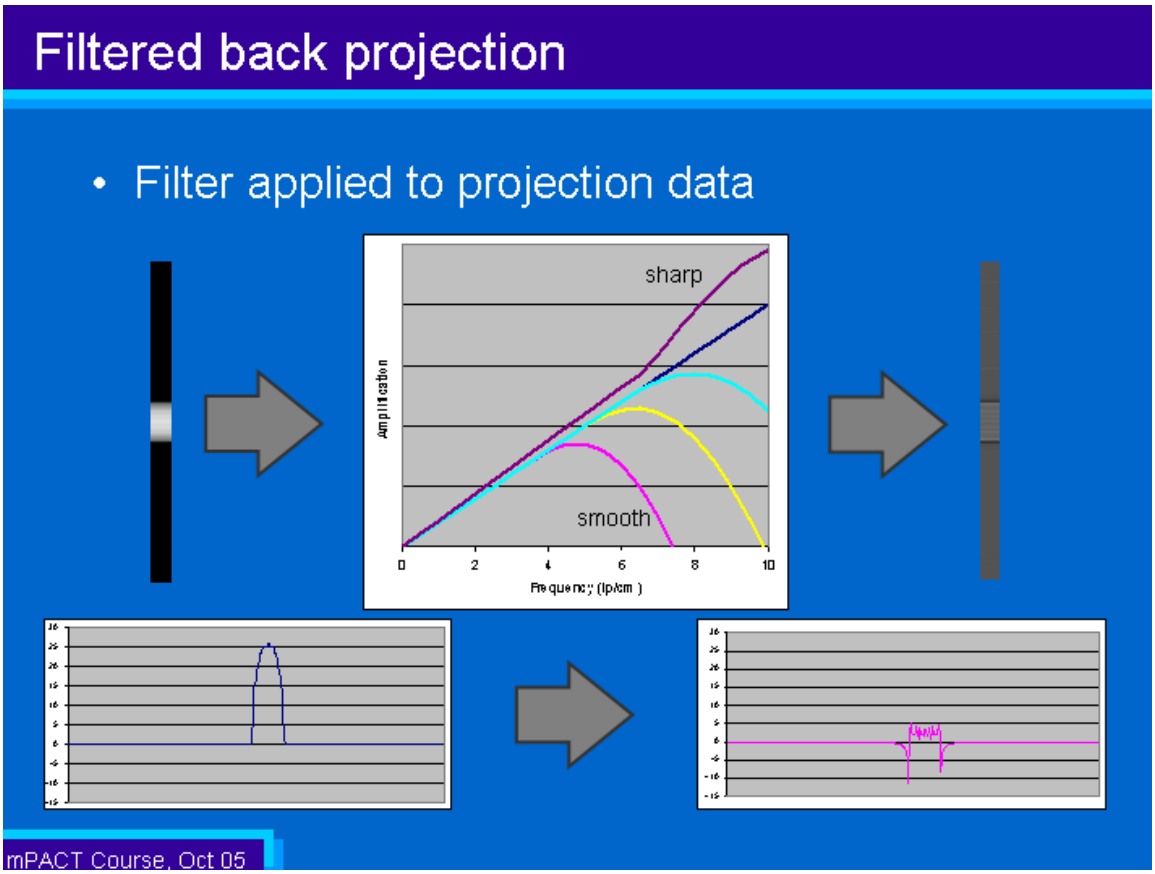

Figure 12 The different curves in the upper graph depict different possible filters in the frequency domain, where the smooth filters attenuates the higher frequencies, while the lower emphasizes the higher frequencies (Weston 2007).

A smoothing filter will not only smooth out the noise, but also the structures, resulting in a more blurry image (See Figure 13 and Figure 14, to the left).

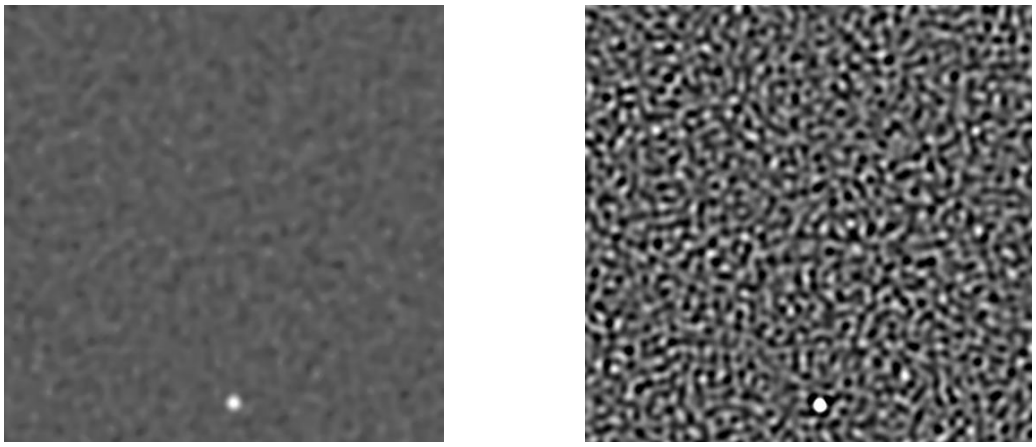

Figure 13: An image of a small wolfram carbid with a 0,28 mm diameter taken from the Catphan 600 Phantom (The Phantom Lab, USA). The image to the left is reconstructed with a soft filter, while the image to the right a sharp filter.

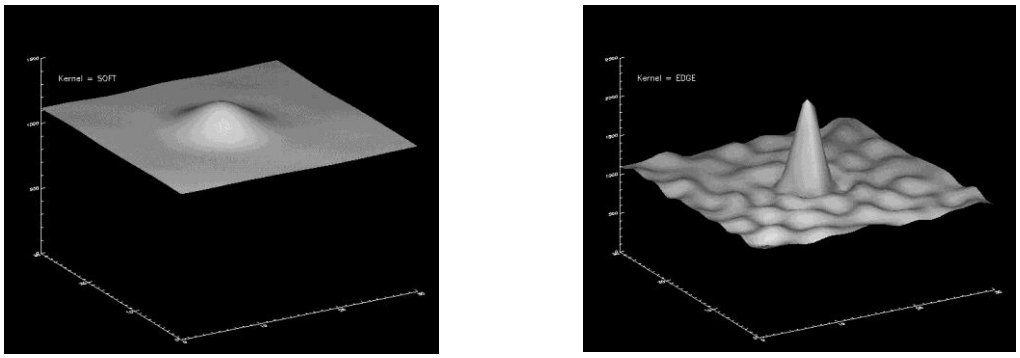

Figure 14: An illustration of how a small wolfram bead will be reproduced using a soft reconstruction filter (left) and a sharp reconstruction filter (to the right).

Filters available for the CT-scanner used in this study, Siemens SOMATOM Definition AS+ is shown in Table 1.

Table 1: Available filters for body CT scan at the Siemens SOMATOM Definition As+. The filter sharpness is defined by the number: The higher the number, the sharper filter.

Filter	Description
10	Very smooth
18	Very mooth
20	Smooth
25	Smooth++
26	HeartView smooth
30	Medium smooth
31	Medium smooth+
35	HeartView medium
36	HeartView medium
40	Medium
41	Medium+
45	Medium
46	HeartView sharp
50	Medium sharp
60	Sharp
70	Very sharp
75	Very sharp
80	Ultra sharp

2.3.2 ITERATIVE RECONSTRUCTION

In iterative methods a A x B matrix which represent pixel values is filled with arbitrary values. Next, an iterative procedure is used to gradually change the values, so they correspond with the values from the projection profiles (see Figure 15 for illustration). For each measured projection profile, the following question is asked: how can the pixel values in the matrix be changed in order to make them consistent with this particular measurement?

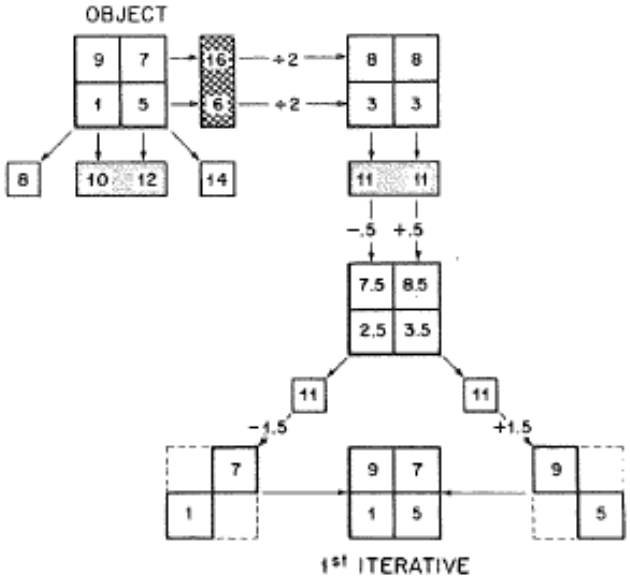

Figure 15: A simple illustration of the principles behind iterative techniques (Curry, Dowdey et al. 1990).

Iterative reconstruction has been available for many years (Webb and Flower 2012) but has not been clinically applicable due to the complex and time consuming calculations. However, the recent years major developments has been done on this method, making the reconstruction method far less time consuming, and today, all vendors have a version of various iterative reconstruction methods.

2.3.2.1 Sinogram Affirmed Iterative Reconstruction (SAFIRE)

The CT scanner used in this study, Siemens SOMATOM Definition AS+® (Siemens Medical Systems, Germany), uses a combined reconstruction algorithm, a mix of FBP and iterative techniques. First, the raw data, the projections, are reconstructed by a traditional filtered back projection (step 2 in Figure 16) Next, this back projected image is subject to a forward projection (step 3 in Figure 16). In this way, the image from the filtered back projection serves as a virtual patient, and the new forward projections as virtual raw data. By comparing the virtual raw data set with the measured raw data set, the differences can be identified and reconstructed using a filtered back projection (step 5 and 6). This "difference-filtered back projected image" is then used to correct the previous one, and an updated image is obtained. This is roughly what happens in the first of two loop mechanisms in the sonogram affirmed iterative reconstruction, SAFIRE (See Figure 16 and left in Figure 17). In the second loop (see Figure 17 to the right), model-based noise detection and subtraction is performed in the image domain, followed by comparison with previous images to ensure convergence of the iterative

process. The first loop mainly corrects for artifacts rising from the inexact nature of filtered back projection, and is only activated if artifact correction is needed, due to the fact that it is a time-consuming process. The amount of artifacts can be estimated from the acquisition parameters set (Grant 2013).

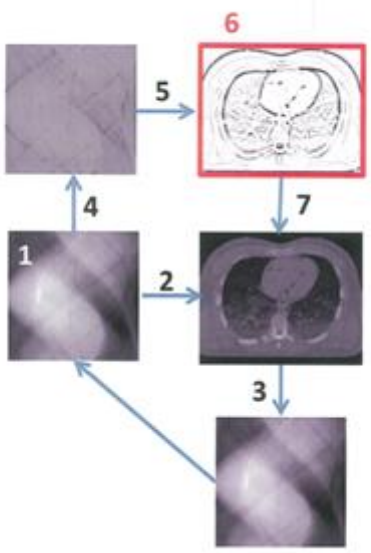

Figure 16: The figure gives an overview of the different principal steps in an iterative technique. 1) Raw data is acquired (sinogram). 2) An initial FBP image is reconstructed. 3) The FBP image is forward projected. 4) The difference between raw data set 1 and 3 is calculated. 5) This difference-raw data set is reconstructed and subtracted from the initial FBP (6 & 7).

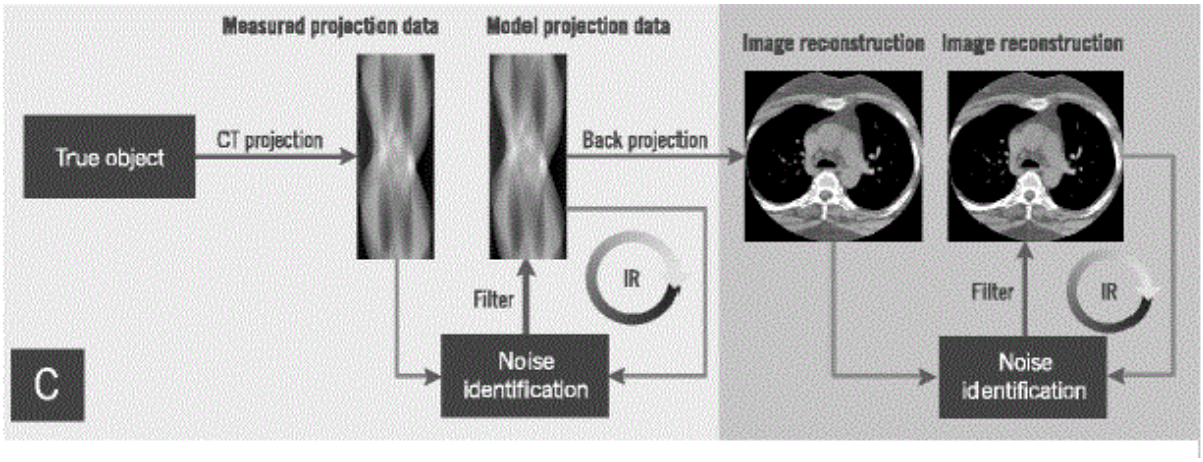

Figure 17: The SAFIRE algorithm iterates directly on the raw data material to the left as described in detail in figure 8 (loop 1). In loop 2 (to the right) model based noise detection and subtraction is performed in the image space, where noise is removed through a statistical optimization process

The SAFIRE algorithm has 5 strength levels which all can be combined with the various filters available at the scanner. When using iterative techniques in addition to filter, the

filter name changes from e.g. B20 (pure FBP) to I20_x, where x stands for the iterative strength level.

When increasing the iterative strength the noise is reduced. However, a so called blotchy appearance is often experienced by the human perceivers at the highest iterative level 4 and 5 (Yang, Yan et al. 2013).

2.4 IMAGE QUALITY

Image quality can be described as the effectiveness with which the image can be used for its intended task (ICRU 1996). The main factors affecting the visibility of lesions in an image are noise and blurriness (poor resolution). A large amount of noise will generally reduce the contrast in the image making low-contrast details less visible, while blurring affects the visibility of anatomic details and small objects, reducing the spatial resolution.

2.4.1 SPATIAL RESOLUTION

During the scanning step of the image-forming process blurring is produced by the finite size of both focal spot and detector (Sprawls 1992). A ray is the segment of an X-ray beam defined by the size of focal spot and detector. If this "effective ray" is wider than the detail to be imaged, the image will be blurred. Another aspect which results in blurring is the size of the voxels. As mentioned earlier, a voxel will only give one single HU number. Variations within a voxel cannot be seen. Therefore, the larger the voxels are, the more blurry the image will be, resulting in a poorer spatial resolution (See Figure 18).

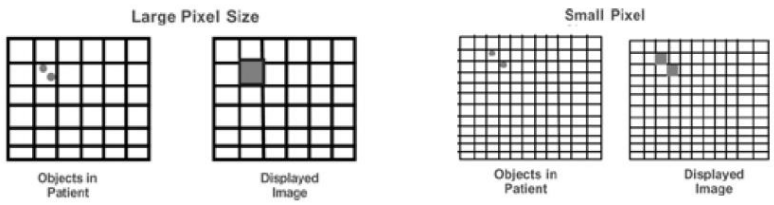

Figure 18: With large pixel sizes (voxels) small details may fall into the same pixel and cannot be separated in the image (Romans 2013).

Roughly, three parameters can be adjusted prior to the scan to control voxel size, and consequently the ability to see small details: field of view, matrix size and slice thickness (see Figure 5 in section 2.2).

During the image processing step the reconstruction filter will strongly influence the degree of blurring of the image.

2.4.2 NOISE

Noise is caused by the variation in attenuation coefficients between the individual voxels and can in its simplest way be defined as the standard deviation of the HU values within a chosen region of interest in a homogeneous material, for instance a water phantom. Ideally, two voxels of identical tissue would result in identical attenuation coefficient values. However, the real situation is different. Due to stochastic variation, the homogeneous object imaged will look structured, or snowy. See Figure 19.

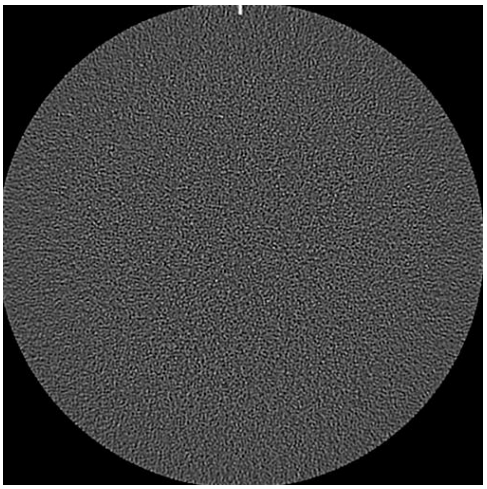

Figure 19: CT scan of a homogenous part of a Catphan phantom.

Since noise is caused by stochastic variation, a good way of reducing this variation is by reducing the randomness of the data, which in this situation means increasing the number of X-ray photons absorbed for each voxel (see Figure 20). During the scanning process when the raw data is recorded, noise reduction can be achieved by adjusting two different parameters:

1) By increasing the mAs value. When increasing the current-time product, the photon fluence will increase, resulting in more photons per voxel. The noise when defined as the standard deviation of the HU values will be reduced as $1/\sqrt{\text{mAs}}$ (Curry, Dowdey et al. 1990). However, increasing the photon fluence will also result in higher dose to the patient.

2) By increasing the voxel size. A larger voxel will intercept and absorb more photons, reducing the statistical variance. Nevertheless, a larger voxel will reduce the spatial resolution.

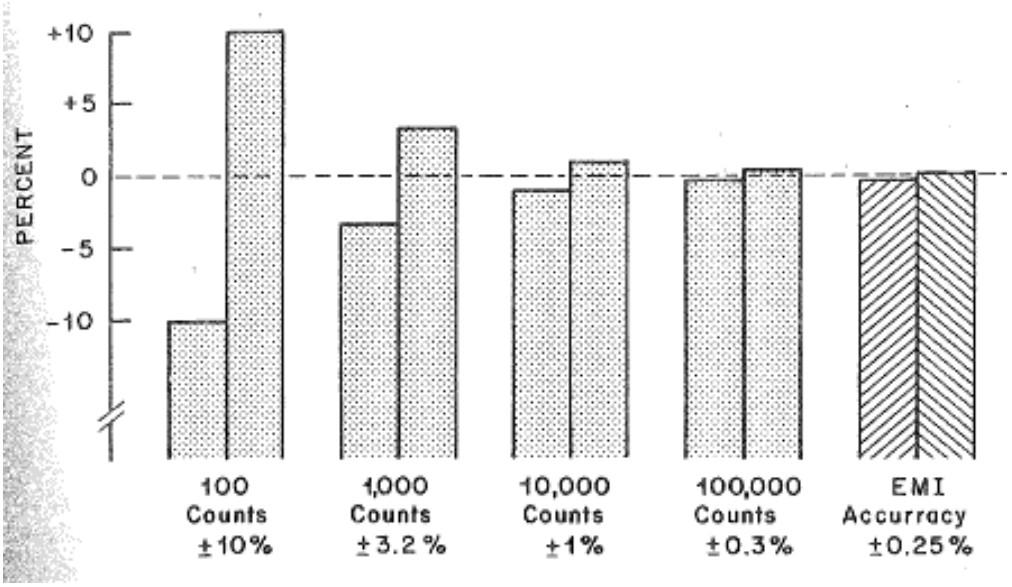

Figure 20: As number of photons (counts) to detector increase, the statistical fluctuations (noise) decrease(Curry, Dowdey et al. 1990)

During the image reconstruction process, applying a smoothing filter will also reduce the noise. But, when improving the noise in an image the spatial resolution gets reduced (Sprawls 1992). However, according to Falck *et al*, the use of iterative reconstruction techniques does not seem to influence the spatial resolution while reducing the noise (von Falck, Bratanova et al. 2013).

2.5 EVALUATION OF IMAGE QUALITY

Both the spatial resolution and the contrast can be directly evaluated through the use of phantoms, specially designed objects with modules containing details that can be evaluated by the used e.g. low contrast visibility and spatial resolution.

Spatial resolution can be evaluated by counting numbers of visible aluminum line pair groups, starting with the line pair group with lowest spatial resolution of 1 lp/cm (line

pair per cm) marked with an orange arrow in Figure 21. (Laboratory 2006; Eldevik, Nordhoy et al. 2010).

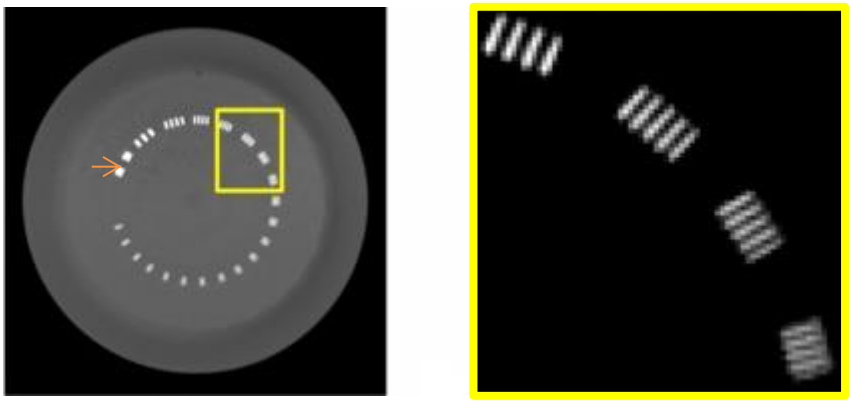

Figure 21: An image taken from the Catphan phantom. The spatial resolution can be subjectively evaluated by counting the number of visible line pair groups. The spatial resolution is given as line pairs per cm (lp/cm).

The visibility of low-contrast details is another aspect of image quality. In for instance the Catphan® phantom, there is a low contrast module containing circles with various nominal contrast levels and with decreasing diameter (See Figure 22). The low-contrast resolution can be defined as the diameter of the smallest low-contrast detail visible at a given contrast level (Webb and Flower 2012). The low contrast resolution is influenced by e.g. the noise level, but also the spatial resolution (Goodenough and Weaver 1984; Webb and Flower 2012).

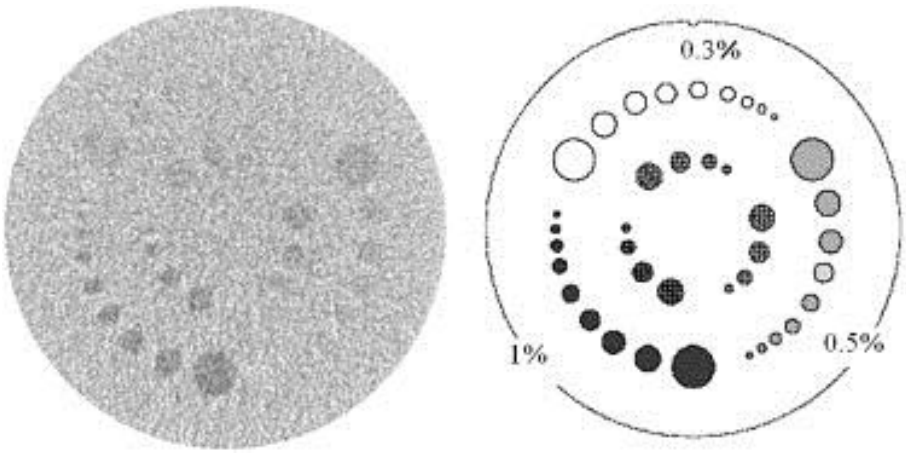

Figure 22: Low contrast resolution module from the Catphan phantom. The module (the figure to the right) contain circles of varying contrast and size. The darkest circles have a contrast of 1% compared to the background, the grey of 0,5 % and the white of 0,3 %. The figure to the left: A CT scan of the low contrast resolution module.

However, even though these methods are relatively easy to perform and interpret, they are time consuming and subject to personal viewing criteria and viewing conditions.

2.5.1 OBJECTIVE IMAGE QUALITY MEASUREMENTS

More objective methods of evaluating the visibility using these detailed phantoms are by calculating the Modulating Transfer Function (MTF) and Point Spread Function (PSF) to evaluate the spatial resolution and to calculate Contrast-To-Noise Ratio (CNR) for the low contrast circles. Also the calculation of Signal-To-Noise ratio is objectively calculated and used as a quantified indicator on image quality (Webb and Flower 2012; Chang, Lee et al. 2013; von Falck, Bratanova et al. 2013) .

2.5.1.1 SNR and CNR

An SNR can in CT be defined as (Webb and Flower 2012; Chang, Lee et al. 2013):

$$SNR = \frac{\mu}{\sigma_{\mu}}$$

Equation 2: Signal-To-Noise Ratio. μ is the reconstructed attenuation coefficient for a given area, while σ_{μ} is the standard deviation in the same area.

As attenuation coefficients are rescaled and given in Hounsfield units before being displayed on the monitor, a more practical implementation of SNR measurements used is (von Falck, Bratanova et al. 2013):

$$SNR = \frac{HU_{average}}{\sigma_{HU}}$$

Equation 3: $HU_{average}$ is the average pixel value given in Hounsfield units in a chosen region of interest. σ_{HU} is the standard deviation of the pixel values within same region of interest (or noise, as simply defined in section 2.4.2).

The Contrast-To-Noise ratio can be defined as (Winklehner, Karlo et al. 2011)

$$CNR = \frac{HU_{ROI1} - HU_{ROI2}}{\sigma_{background}}$$

Equation 4: HU_{ROI1} and HU_{ROI2} are average pixel values in two different chosen regions of interest. $\sigma_{background}$ is the standard deviation of the pixel values in the background, where background may i.e. be defined as the ROI with lowest average pixel value.

The CNR plays a certain role when it comes to detecting objects of inherent low contrast as illustrated in Figure 23 . Low contrast objects with a high noise level will generate a low CNR value which results in reduced visibility of the object as marked in the green boxes in Figure 23.

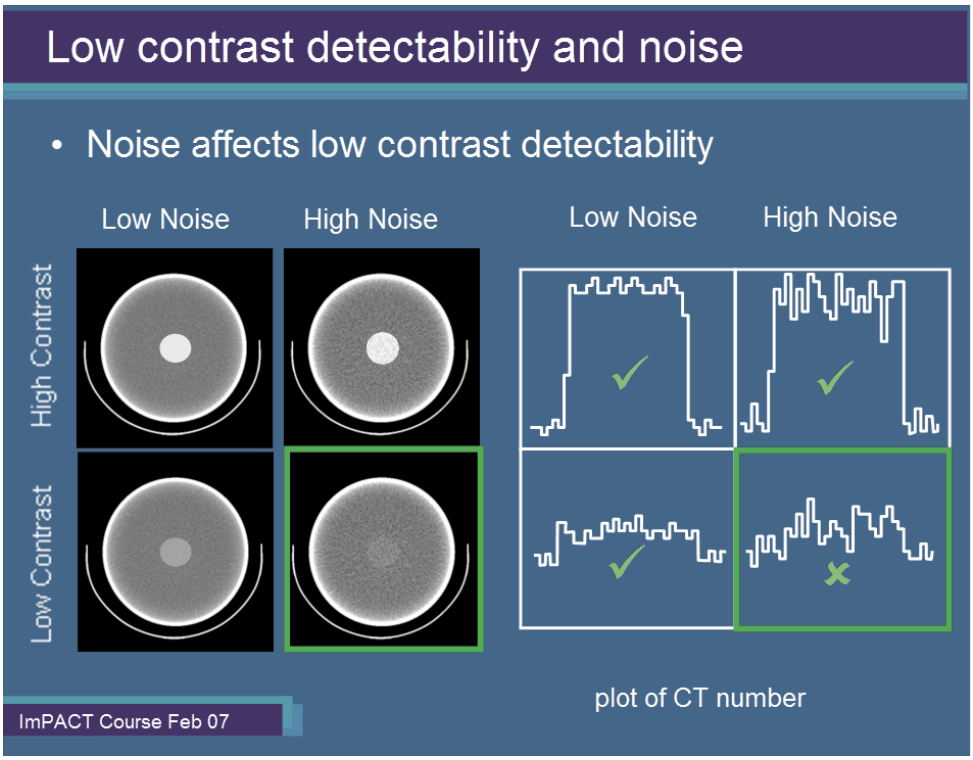

Figure 23: With high inherent contrast, the object is clearly visible also with a high noise level. At low inherent contrast the object visibility is significantly reduced when the noise level is high (Edyvean 2007).

2.5.1.2 Modulating Transfer Function

The modulating transfer function (MTF) characterizes how well the system can image information at the different spatial frequencies. The MTF is calculated from the Fourier Transform of the Point Spread Function, or the edge response of the square-wave response (See Figure 24 for illustration of the two latter terms). However, the concept of modulating transfer function is best visualized in Figure 25.

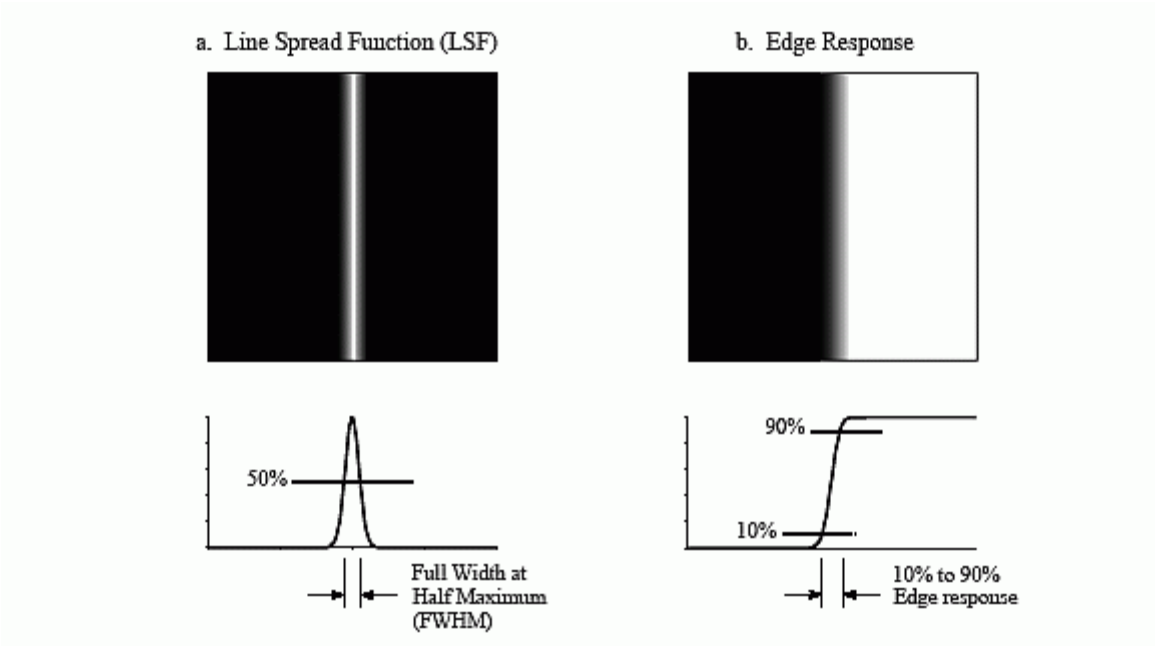

Figure 24: Line spread function and edge response. The line spread function is the derivative of the edge response. The width of the LSF is often expressed by the FWHM, while the edge response is often characterized by the distance between 10% value and 90% value (with 100% value being the value in the white area) (Smith 2002).

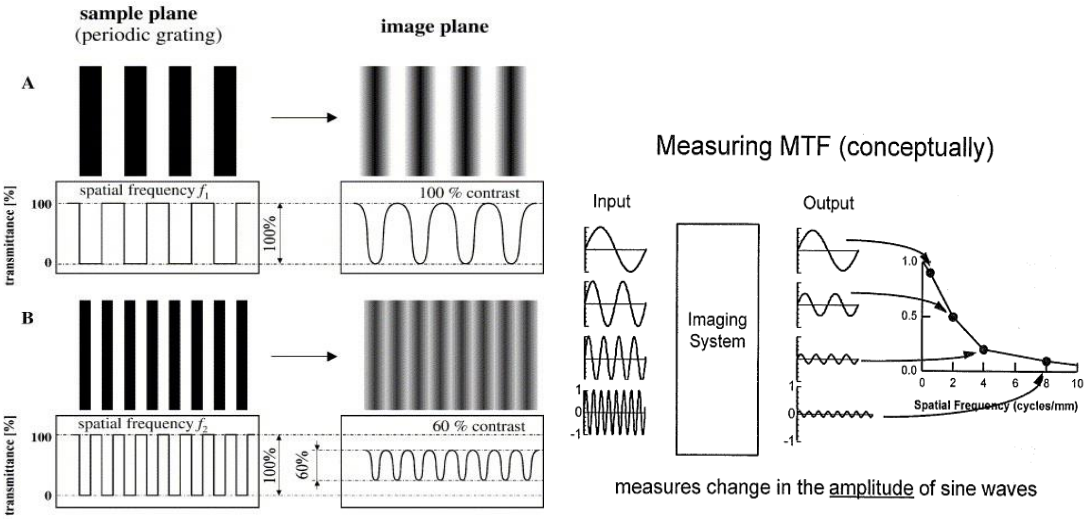

Figure 25: The figure illustrates how the amplitude of the spatial frequencies is modulated. The higher spatial frequencies, the more are the spatial sine wave amplitude modulated. The MTF curves are a plot of these modulated amplitudes as a function of spatial frequency (Nishikawa 2013).

2.5.1.3 The Point Spread Function and the Line Spread Function

The point spread function is a way of measuring the sharpness in an image. When imaging a phantom containing a small bead of high density and plotting the relative intensity as a function of distance from the center of the bead, a two dimensional plot of the intensity can be obtained (see Figure 26).

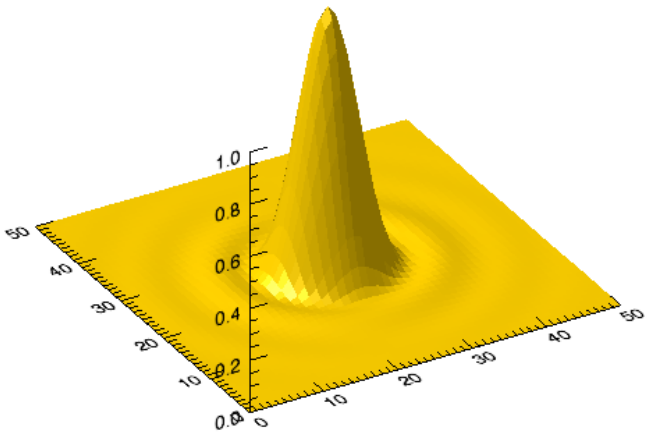

Figure 26: An example of a two dimensional plot of the point spread function (Smith 2009).

If assuming that the PSF is a 2D Gaussian function with standard deviation σ, a projection of this function on one of the main axis will form a 1D Gaussian with identical standard deviation. Under these assumptions, it is possible to determine the Full-Width-Half-Maximum (FWHM) of the Line Spread Function, and use this value as a measure of the image sharpness (Eldevik, Nordhoy et al. 2010).

2.5.1.4 Noise analysis

One approach to measure the noise level is by imaging a homogenous material, e. g. water phantom, and calculating the standard deviation of the HU values within a region of interest. However, the standard deviation only gives information on how much the HU values varies within the chosen region, not how it is structured (See Figure 27) . To gain information on the spatial distribution of the noise, a Noise Power Spectrum can be calculated.

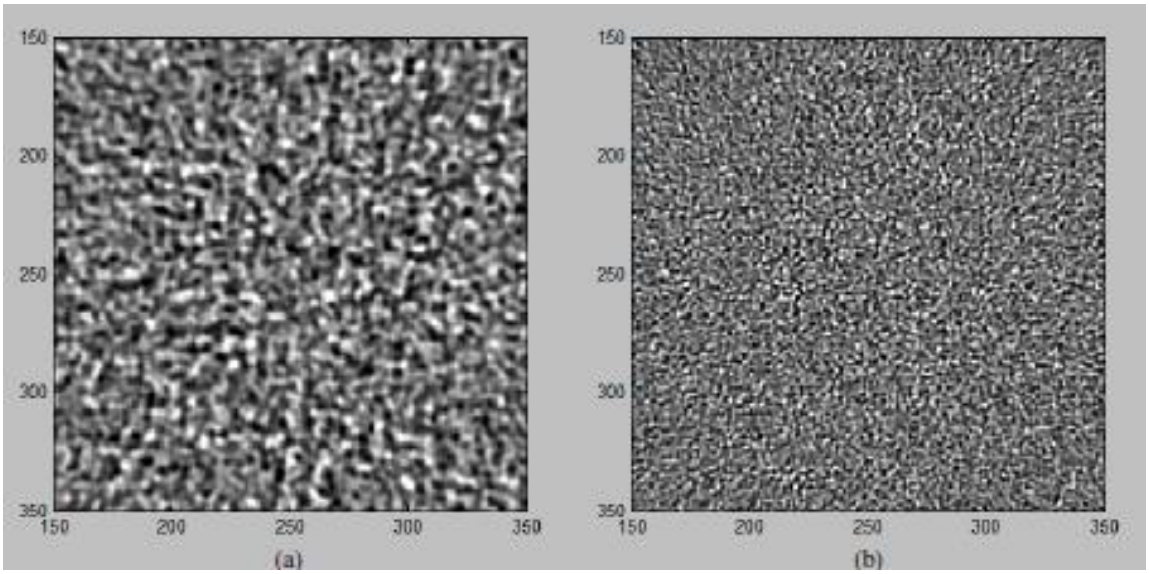

Figure 27: The two noise-images have the same pixel standard deviation, but the image to the left, taken with a very soft filter has a much coarser appearance and appears noisier (Boedeker, Cooper et al. 2007).

The Noise Power Spectrum shows how the noise is distributed as a function of spatial frequency. An image dominated by high-frequency noise will have a finely grained structure (figure 24 b), while an image containing mostly low-frequency noise will look patchier/course (figure 24 a), even though the standard deviation (the amplitude of the noise) is the same (Boedeker, Cooper et al. 2007). See Figure 28.

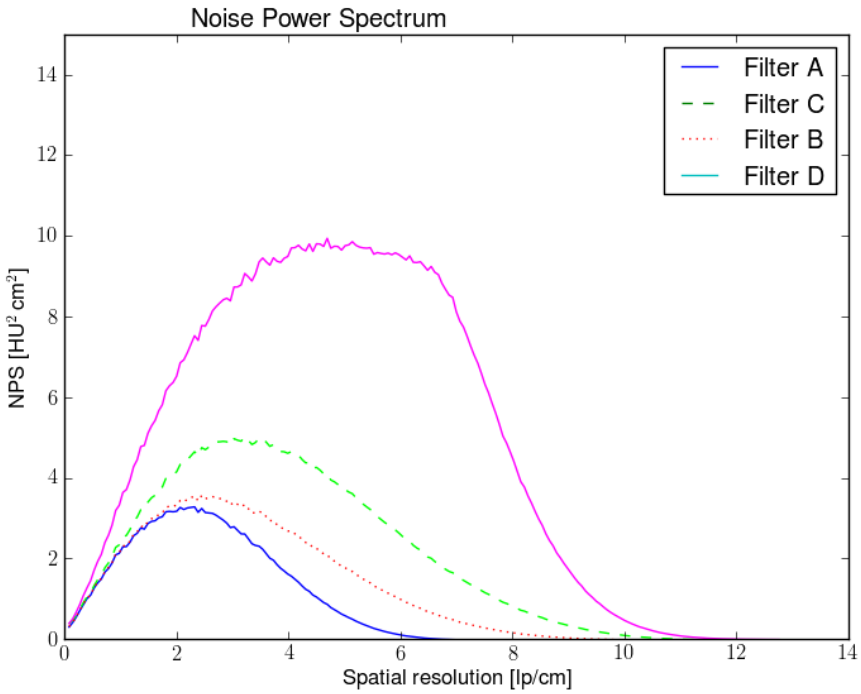

Figure 28: NPS curves for 4 different reconstruction filters. The filters have increasing filter sharpness (A smoothest, D sharpest) which directly have a directly impact on the noise distribution. The sharper a filter is, the more finely distributed will the noise be (leading a shift to the right in spatial frequency domain).

2.6 Optimization

According to the regulations of the Norwegian Radiation Protection Authority (NRPA 2013) § 38 all CT protocols should be optimized: *"Optimization includes choice of method, equipment, apparatus, evaluation of diagnostic information, practical feasibility of the examination in addition to evaluation of working techniques and radiation dose to the patient".*

When maintaining adequate image quality i.e. good enough to be used for its intended task at as low dose as reasonably achievable, the protocol can be approved as optimized. There are several challenges connected to optimization projects. Ideally patient groups should be used when testing out the lower dose alternatives, followed by subjectively interpretation of the image quality by radiologists. However, use of patients in these sorts of studies requires approval from the ethical committee. In addition subjective interpretation by radiologists is very time consuming. As a substitute for real patients, anthropomorphic (humanlike) phantoms containing synthetic organs can be used. However, it can be questioned how humanlike they really are.

Often non-anthropomorphic phantoms like the Catphan phantom described previously are used as an initial part of an optimization process, as it offers the opportunity to quantify physical image quality parameters like noise, contrast resolution and spatial resolution.

3 MATERIALS AND METHODS

In this study the optimization potential of a specific protocol, thorax-abdomen/pelvis has been investigated. All scans were performed on a Siemens SOMATOM Definition AS+ (Siemens Medical Systems, Germany). The following parameters where held constant for all the scans:

- The detector configuration and slice thickness, 128 x 0.6 mm.
- Beam energy, 100 kVp

And following parameters where varied:

- mAs
- filter
- iterative strength

The aim was to find lower dose alternatives at 50% dose level, 62,5% dose level and 75% dose level which fulfilled following criteria:

- Similar noise level as the nominal full dose setting (100%)
- Similar spatial resolution as the nominal full dose setting

When performing a typical thorax-abdomen/pelvis examination, a raw data scan ranging from the shoulders to the start of the legs is performed. The scan region can be seen in Figure 29.

Figure 29: The scan region visualized by the topogram taken prior to the CT-scan. The scan region ranges from the shoulders to the start of the legs when performing a thorax-abdomen/pelvis examination.

In the current scan protocol the raw data is then reconstructed with two different reconstruction filters in the thorax area (the area marked with a purple box in Figure 30), one soft filter for mediastinum, I31_3, and one sharp filter for lungs, B70 (no iterative techniques applied). The abdomen/pelvis area (the area marked with a red box in Figure 30) is reconstructed with the soft filter I30_1.

Figure 30: The figure illustrates the different reconstructed volumes in a typical thorax-abdomen/pelvis scan on an anthropomorphic phantom. The purple box is the lungs and mediastinum volume, and is reconstructed with a sharp filter for viewing the lungs and a soft filter for viewing the mediastinum. The abdomen area marked with a red box and is reconstructed with a soft filter.

In today's protocol, a quality reference mAs of 240 is used when scanning the raw data set. Due to the dose modulation, the effective mAs-value will vary along the z-axis of the patient (see Figure 31), reaching its highest value in the pelvic area and lowest value in the lungs.

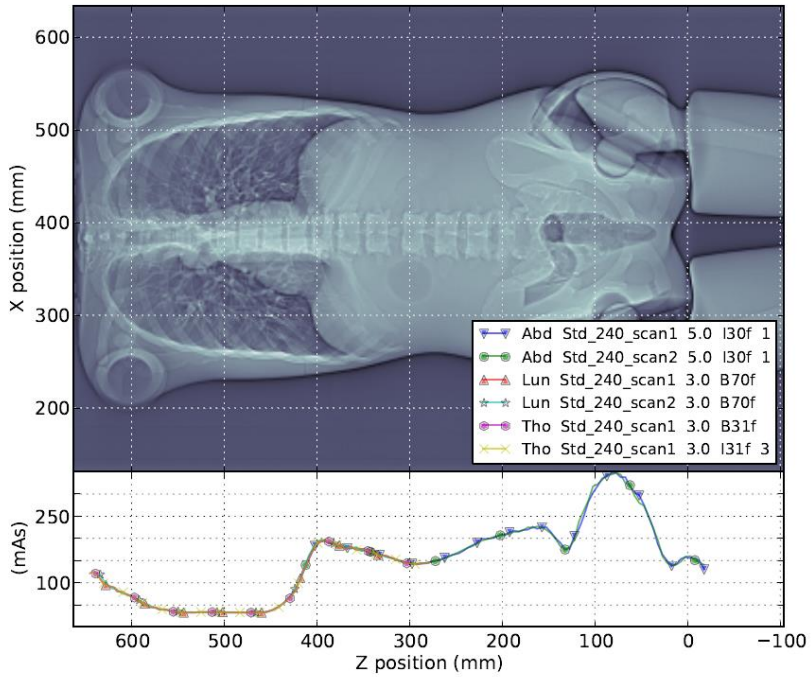

Figure 31: A mAs plot of an anthropomorphic phantom used in this study with a quality reference mAs of 240. The plot illustrates how the dose (mAs) is lowest in the lungs, increases in the abdomen and reaches its peak in the pelvic area. The mAs curve is slightly lower for the "slim" anthropomorphic phantom than initially found from patients scan.

Some CT scans of normal, average-weighing patients were investigated in order to collect nominal mAs-values in the lungs and in the abdomen area to use as a reference for all objective measurements performed in this study. The nominal parameters shown in Table 2 were selected for the lung, the mediastinum and abdomen:

Table 2: The nominal parameters used in the study.

Anatomic region	Reconstruction parameters	mAs-value
Lung	B70	40mAs
Mediastinum	I31_ 3	40 mAs
Abdomen	I30_1	400 mAs

The alternative parameters where explored for the different regions as shown in Table 3.

Table 3: The different lower dose alternatives explored in this study

	Reconstruction filters and iterative strength			Dose	
Anatomic region	**Nominal reconstruction parameters**	**Alternative Reconstruction filters**	**Alternative Iterative strengths**	**Nominal mAs-values**	**Alternative mAs-values**
Lung	B70 (FBP)	70	1 2 3 4 5	40mAs	20 mAs 25 mAs 30 mAs
Mediastinum	I31_ 3	31 40 41	4 5	40 mAs	20 mAs 25 mAs 30 mAs
Abdomen	I30_1	30 31 40 41	2 3 4 5	400 mAs	200 mAs 250 mAs 300 mAs

For the mediastinum the neighboring filters 40 and 41 were tried out as alternatives to 31.

For the 70 filter used in the lung reconstruction, no sharper filter was available when applying iterative techniques. Therefore, only a higher iterative strength in combination with lower dose where tried out for the lungs. Using a smoother filter in the lungs was not an alternative, as sharpness must be contained to obtain diagnostic good image quality.

For the abdomen area, the filters 31, 40 and 41 where examined for all different dose levels.

The best lower dose alternatives for each anatomic region where then found through different image quality analysis step (see Figure 32), starting with analysis on a Catphan

phantom. For e.g. abdomen (see Table 3), there is in total 48 different lower dose alternative settings. To efficiently narrow down the options and sort out which alternatives that fulfills the noise criteria and spatial resolution criteria, an objective noise and spatial resolution analysis using the Catphan phantom were performed (step 1 in Figure 32).

The scan alternatives fulfilling these criteria where then applied to CT scans of an anthropomorphic phantom, where the image quality were evaluated by measuring SNR and CNR (step 2 in Figure 32).

The best lower dose alternatives with similar SNR and CNR values as the nominal 100% dose level where sent to radiologists (step 3 in Figure 32).

The radiologist found the best lower dose alternative which could then be further examined on patients scan (not performed in this study).

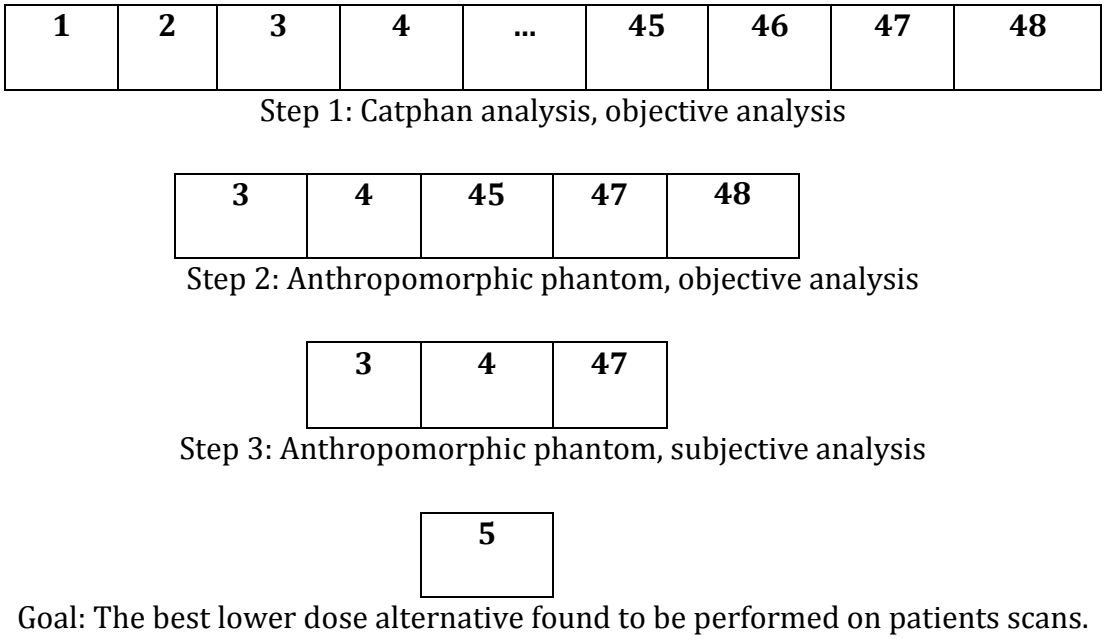

Figure 32: The figure illustrates the elimination process conducted in this study. The numbered boxes illustrate the different scan alternatives available for abdomen. The first step was to analyze the objective image quality using the Catphan phantom. The number of different scan alternatives was narrowed down based on how well the image quality criteria were fulfilled. Step 2: The selected scan alternatives were applied to the anthropomorphic phantom. The best alternatives found from an objective image quality analysis of the anthropomorphic phantom where further examined subjectively by experienced radiologists. The best lower dose alternative and reconstruction filter found by the radiologist can be further analyzed by applying the alternative on patient scans.

3.1 Objective analysis of image quality using a Catphan phantom and PSF Noise

A Catphan® 600 phantom (The Phantom Laboratory, Germany) was used to evaluate image quality at the nominal reference scan parameters and to find similar image quality at lower doses and alternative reconstruction filters. The Catphan phantom (See Figure 33) is a specially designed object used to evaluate image quality for CT. Different tests can be performed, evaluating the homogeneity, the noise level, the point spread function, the Modulation transfer function and the visibility of low contrast details(Laboratory 2006). The evaluation methods of interest in this study were calculation of the point spread function and measuring the noise level.

Figure 33: A photo of the Catphan 600 phantom to the left. To the right: A sketch of the various modules for measuring linearity (CTP404), slice thickness (CTP591), spatial resolution (CTP528), low contrast (CTP515), noise and homogeneity (CTP486) (Laboratory 2006).

To evaluate the spatial resolution in this study, an IDL program called PSF_Noise was used (Eldevik, Nordhoy et al. 2010) . This program measures the PSF of a wolfram carbide bead with a diameter of 0.28mm in section CTP591 of the Catphan phantom (See Figure 33 and Figure 34). The user marks the bead in each image, and the program then calculates the PSF from a pre-defined area around the bead. The full width at half maximum (FWHM) of the PSF is then automatically calculated by approximating the PSF to a Gaussian function (See Figure 35).

a) 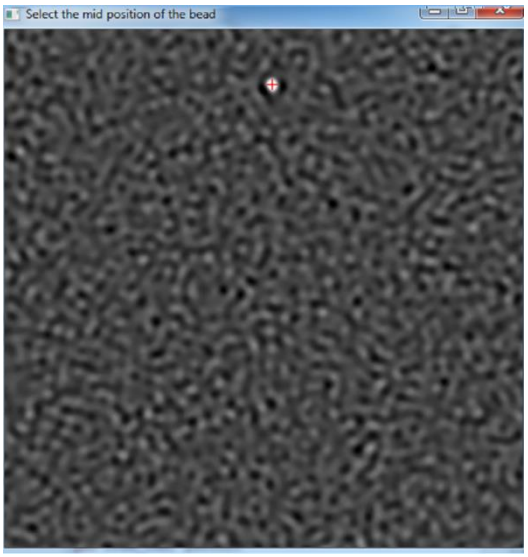

b) 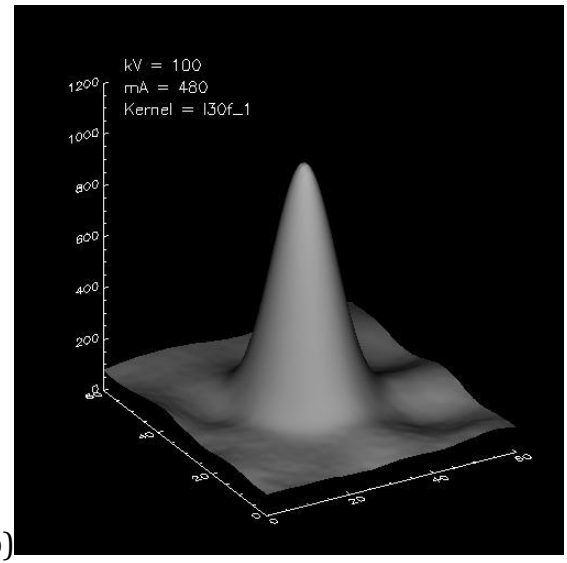

Figure 34: (a) The user manually marks the center of the bead in the image in the PSF_Noise program. The program then uses the pixel values to calculate PSF, LSF and FWHM for the specific image taken at specific scan parameters. (b) The three-dimensional visualization of the Point Spread Function based on the image of small wolfram carbide.

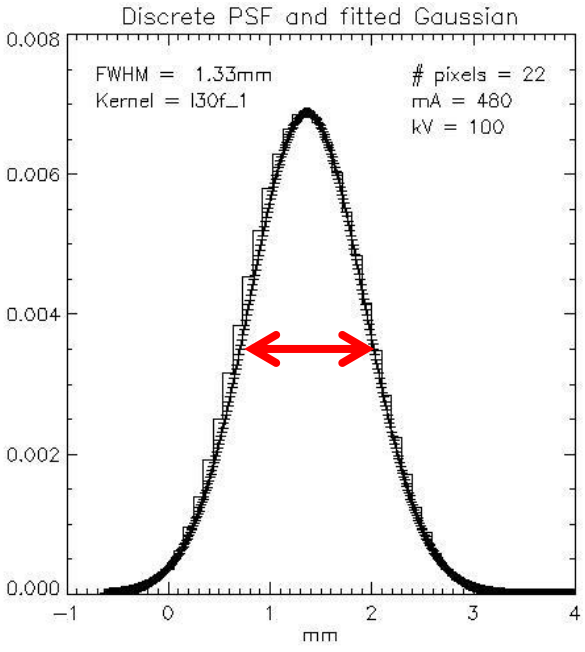

Figure 35: The plotted pixel values from the calculated Line Spread Function and the corresponding fitted Gaussian used to estimate the FWHM of the bead for the given conditions. The red arrow indicates the FWHM.

The same program also calculates the noise. This is done by taking the standard deviation of the HU values in a region of interest of 15 x 15 cm size in a homogenous part of the Catphan phantom, the CTP486 module.

To obtain more detailed information about the distribution of the noise, a Noise Power Spectrum was generated for each setting of mAs/kernel/iterative level.

The properties of the different filters used in this study and the iterative levels were examined and analyzed by making several NPS plots showing:

a) How the noise level and spatial resolution is affected by the filter

b) How the noise level and spatial resolution is affected by iterative strength

c) How the noise distribution changes as a function of mAs, filter or iterative level

To calculate the uncertainty for the FWHM value obtained for a specific mAs/filter/iteration combination, 10 separate scans of the bead where performed without changing the table position, yielding 10 separate raw data sets of the wolfram carbide bead. The images were then reconstructed using the different filter/iteration-combinations and the images were then analyzed one by one in the PSF_Noise program. In this way both uncertainties due to variations in marking the center of the bead in the program and the statistical variation of the pixel values from each raw data acquisition were accounted for.

For the values obtained for the noise uncertainty analysis, 10 adjacent slice locations within the homogenous part of the Catphan phantom, the uniformity module CP468 were used to perform the uncertainty calculations.

The average FWHM values where further used in the resulting graphs with error-bars to be able to verify significant differences.

3.2 Scan of an anthropomorphic phantom.

By analyzing plots of noise versus FWHM for the different combination of mAs/kernel and iterative level, several alternatives to the nominal settings I30_1 - where found at 50%, 62,5% and 75% dose level, which fulfilled the image quality criteria on no loss of/improved spatial resolution, improved or equal noise level.

The selected combinations of mAs/kernel/iterative level found when imaging the Catphan phantom where applied to an anthropomorphic phantom (See Figure 36).

Figure 36: The anthropomorphic phantom used in this study (Kyoto Kagaru, Japan).

The anthropomorphic phantom (Kyoto Kagaru CT Whole Body Phantom, Japan) contains several synthetic vital organs like kidneys, liver, large bowel and skeleton. When scanning the phantom using the current clinical protocol, i.e. nominal quality reference mAs of 240, the phantom attenuates approximately the same amount of radiation as expected of a slim adult patient, i.e. yielding comparable mAs modulation curve as a slim adult patient.

In addition to a CT-scan using a nominal image quality mAs of 240mAs (100% dose), lower dose alternatives were also scanned, that is reference mAs of 180 mAs (75% dose), 150 mAs (62,5% dose) and 120 mAs (50% dose) where taken. The nominal reference scan of 100% dose was reconstructed using filters and iterative levels according to the current scan protocol. The images from the lower dose alternatives where reconstructed with filters with iterative levels found to match the noise level and spatial resolution from the Catphan analysis at given dose reduction level.

Also, reading of mAs values at varies positions along the z-axis of the scans was done, to verify that mAs values for all z-positions where reduced with e.g. 50% when the quality reference mAs was reduced with 50%.

The phantom was not moved between the different scans performed resulting in identical x, y and z – coordinates for all scans.

3.2.1 OBJECTIVE ANALYSIS OF THE ANTHROPOMORPHIC PHANTOM

The average noise level in the homogenous regions inside and outside different anatomic structures where calculated using an in-house-made analysis software in Python (Python Software Foundation version 2.7.3.1, The Netherlands). The program places small regions of interest (ROI) at given coordinates as see in Figure 37, where the average pixel values and the standard deviation in each ROI are calculated. The Contrast-to-Noise ratio (CNR) and Signal-To-Noise ratio (SNR) where calculated by using the following formulas (Heyer, Mohr et al. 2007):

$$SNR = \frac{HU_{average}}{\sigma_{HU}}$$

Equation 5: $HU_{average}$ is the average pixel value found in the region of interest, while σ_{HU} is the standard deviation of the pixel values within same ROI (the noise).

$$CNR = \frac{HU1_{average} - HU2_{average}}{\sigma_{HU2}}$$

Equation 6: $HU1_{average}$ and $HU2_{average}$ is the average pixel values within region 1 and 2. σ_{HU2} is the standard deviation of the pixel values within ROI 2 (the background noise).

The ROI's where placed at the exact same x, y and z coordinate for all scans. Two separate scans of the phantom at each dose reduction level (quality reference mAs of 240 mAs, and lower dose alternatives with quality reference mAs of 180 mAs, 150 mAs and 120 mAs) were taken and used to calculate average SNR and CNR values for each parameter setting with corresponding uncertainty.

For the abdomen area, one ROI was placed in a homogenious region inside the liver, while the other ROI was placed in an homogeneous region outside the liver. Both ROI's were of same size of 18 x 18 mm (see Figure 37).

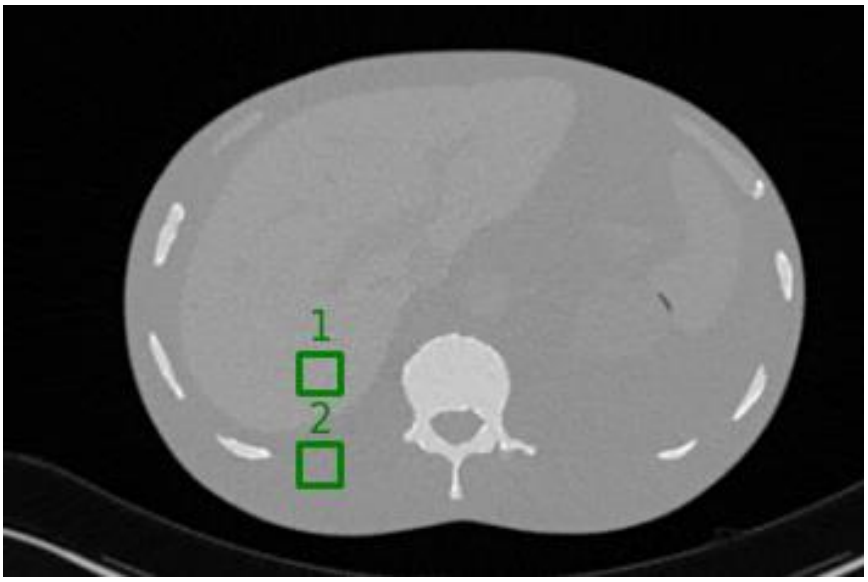

Figure 37: The figure shows a slice from the anthropomorphic phantom marked with 2 different regions of interest used to calculate SNR and CNR, in this case for the liver.

For the mediastinum area ROI number 2 was placed in intermediastal tissue, while ROI number 1 was placed in a lymphnode (see Figure 38) . The ROI's sizes were reduced to fit the size of the lymphnode(12 x 12 mm).

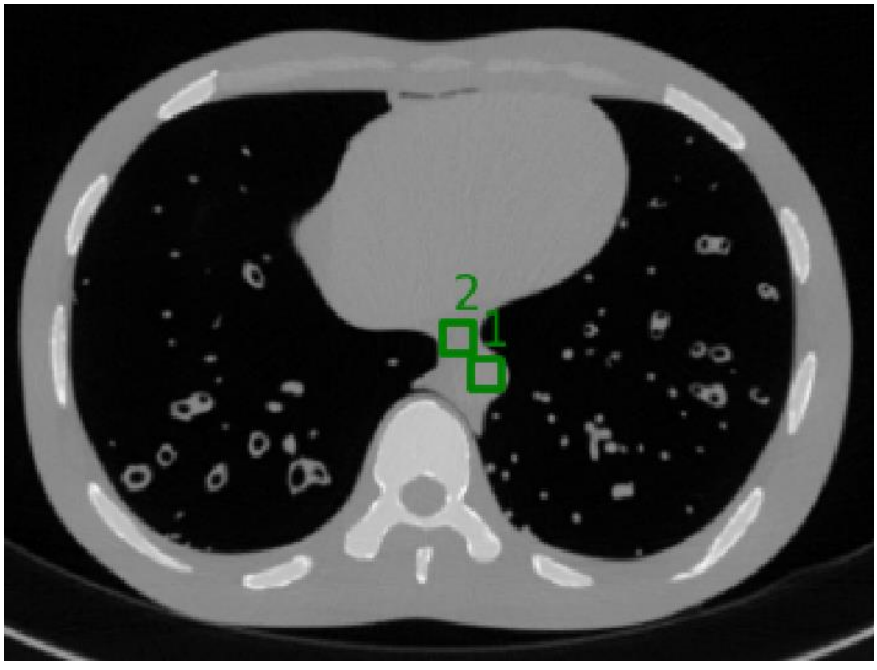

Figure 38: The chosen CT slice of the mediastinum and the position of the ROIs used to calculate the objective image quality parameters SNR and CNR.

The obtained SNR and CNR values where seen in relation to previous results from the Catphan analysis and the best alternatives where then sent to two experienced radiologist for subjective evaluation of the anthropomorphic phantom lower dose options. One experienced gastro radiologist evaluated CT scans of the abdomen part of the anthropomorphic phantom and an experienced thorax radiologist evaluated the CT-scans of the lungs and mediastinum.

3.2.2 SUBJECTIVE ANALYSIS OF THE ANTHROPOMORPHIC PHANTOM

Each radiologist received 4 scans with alternative dose levels, iterative level and filter, in addition to a scan taken at the current reference settings used in the clinic today. The mAs/filter/iterative level for the alternative scans was concealed for the radiologist during the analysis of the different studies.

Both radiologists evaluated the image quality in all the different alternative lower dose scans, comparing it to the reference scan, and tried to give an estimate on whether the image quality could be classified as better, similar or worse than the reference scan.

The radiologist evaluating the image quality in the abdomen based his decisions on how visible he perceived the low-contrast details in the lever compared to the reference image (See Figure 39), the shape of the liver edge, the edge of the pancreas and the separation between the aorta and surrounding tissue.

i) 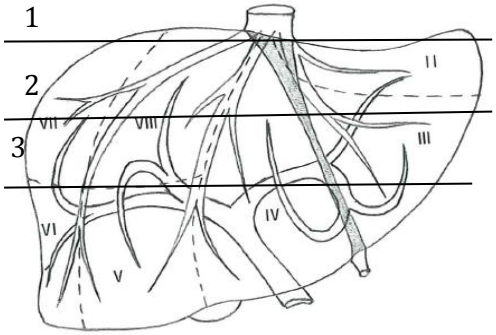

1) 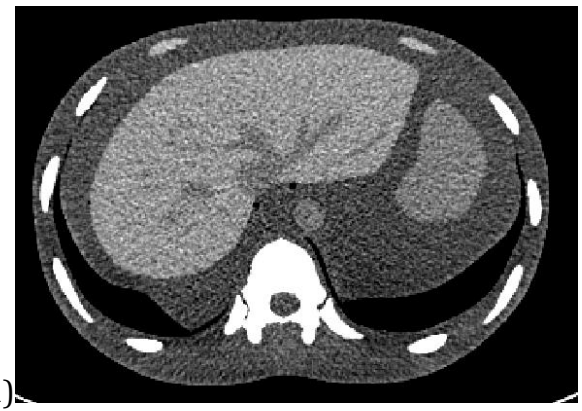

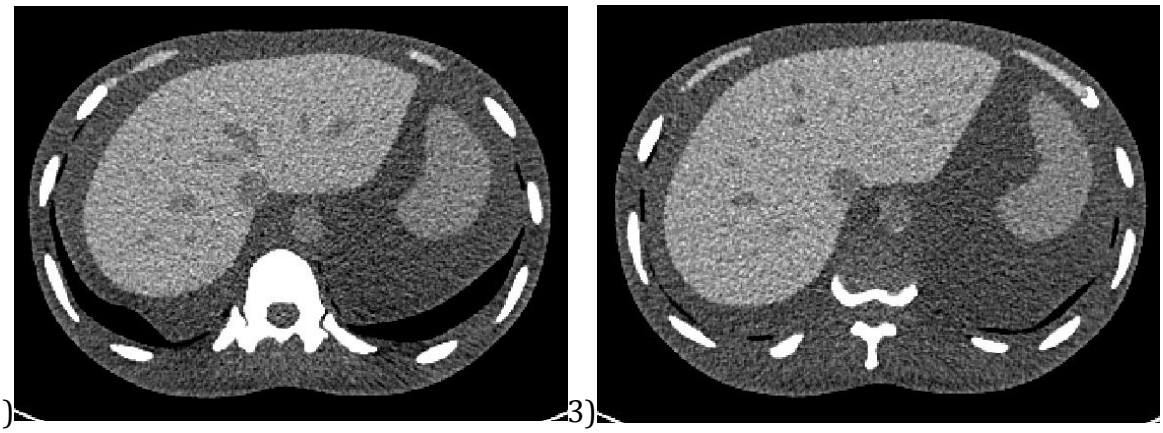

Figure 39: i) A sketch of the liver and its' veins (Merran and Dixon 1991). The three different levels has been marked as 1, 2 and 3. Moving down in the liver, the vessels move outwards and become thinner. How far out these vessels were visible where used as an image quality criteria. The CT images are from the reference setting of 240 mAs, filter I30_1.

The thorax radiologist evaluating mediastinum and lungs concluded that the anthropomorphic phantom missed several vital structures in the thorax, most importantly the lung parenchymal (see Figure 41). The thorax radiologist therefore based his image quality evaluation on the few structures available such as the visual reproduction of the heart and lymph nodes, ribs and muscles.

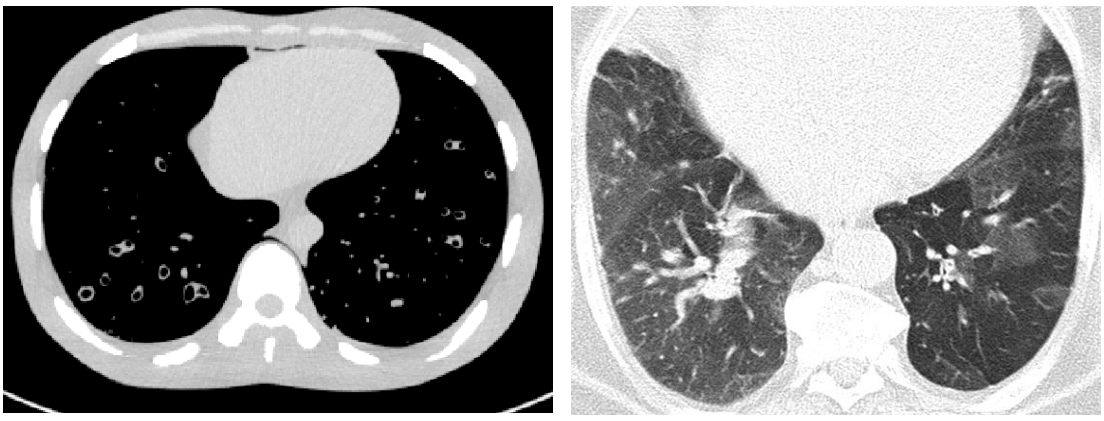

Figure 40: To the left: a CT image of the lung area of the anthropomorphic phantom used in this study. To the right: A scan of the lung area of a human (Castaner, Gallardo et al. 2009)

4 RESULTS

4.1 OBJECTIVE ANALYSIS OF IMAGE QUALITY USING CATPHAN

4.1.1 THE EFFECT OF CHANGING THE RECONSTRUCTION FILTER AND ITERATIVE LEVEL

As expected, the amount of noise in an image increased with increasing filter sharpness. An image taken at 200 mAs with a B30 filter has the same STD of the measured pixel values as an image taken at 300 mAs with a B41 filter (see Figure 41).

With increasing filter sharpness, the spatial resolution generally increases, as expected. There is however no significant improvement in spatial resolution when going from filter B31 to B40, just an increase in noise (see Figure 41 and Figure 42).

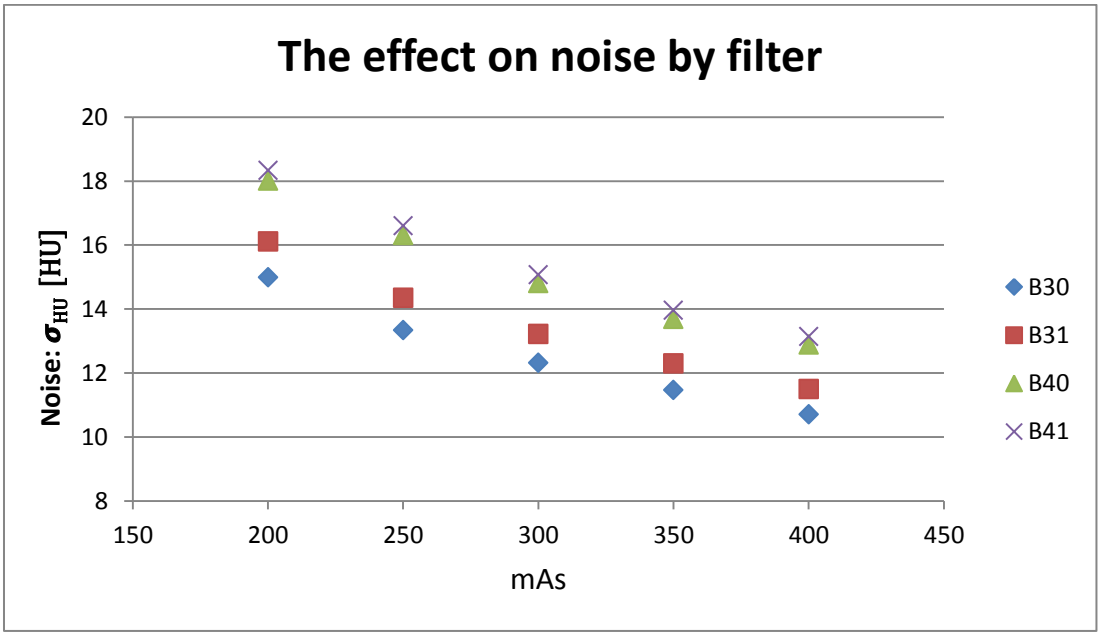

Figure 41: The graph shows the relationship between noise and filter, with increasing mAs value along the x-axis and increasing noise level along the y-axis. The noise decreases approximately $1/\sqrt{mAs}$, as expected.

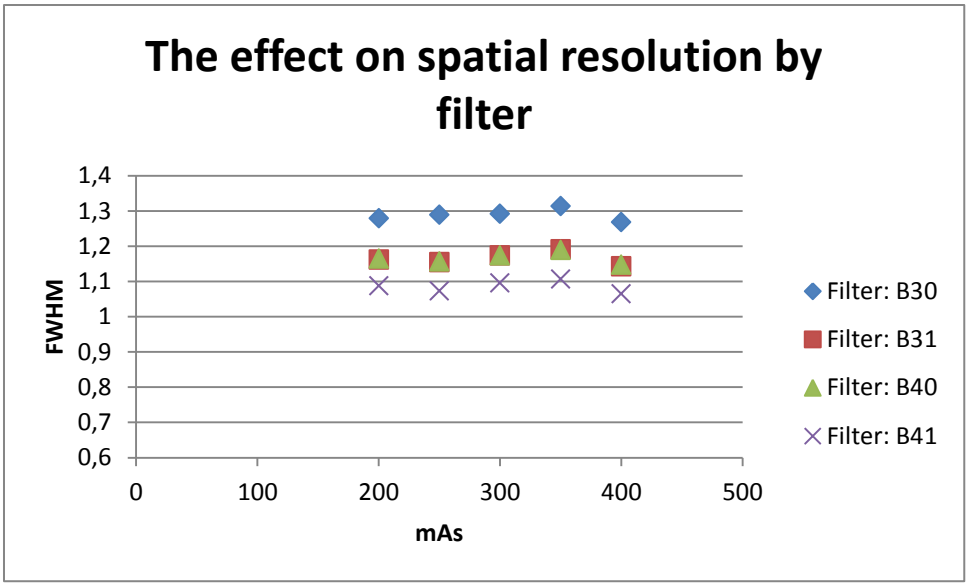

Figure 42: The graph shows how the FWHM is altered when changing the filter. The lower the FWHM value, the better the spatial resolution. There is no correlation between FWHM and mAs.

The noise images taken from the homogeneous CTP 486 module in the Catphan phantom, reconstructed with a B30 filter (FBP, no iterations) at 400 mAs has approximately the same noise level as an image taken at 200 mAs reconstructed with I30_2 at the same slice in the Catphan phantom as seen in Figure 43. Correspondingly, an image taken with iterative level 3 at 400 mAs has approximately the same noise level as an image of the same slice with iterative level of 5 at 200 mAs.

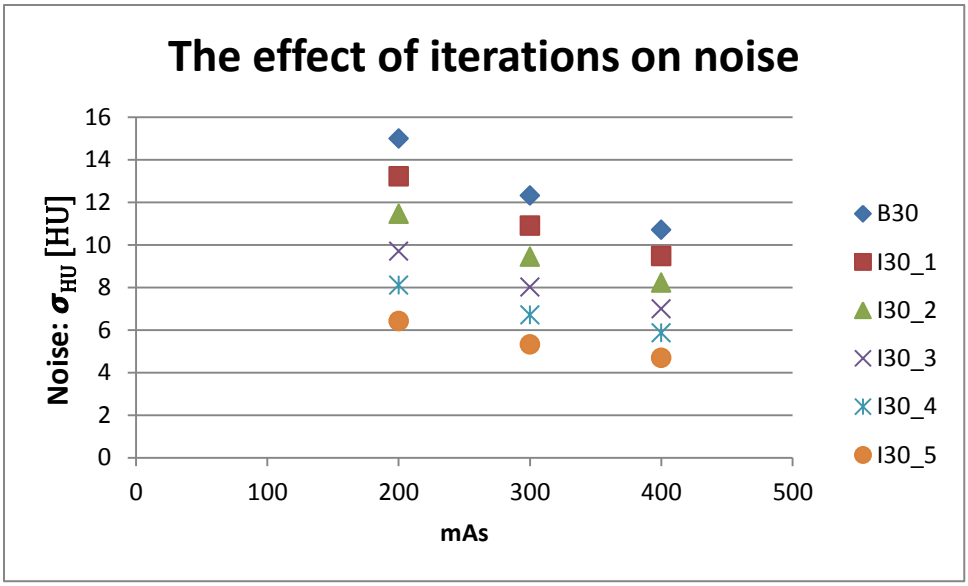

Figure 43: The graph shows how the noise is decreased by each iterative level, in addition to the general reduction of noise when increasing the mAs value. The figure also demonstrates how the noise level for e.g. B30 at 400 mAs is similar to I30_2 at 50% dose level, 200 mAs.

The spatial resolution is not significantly altered with increasing iterative level as shown in Figure 44).

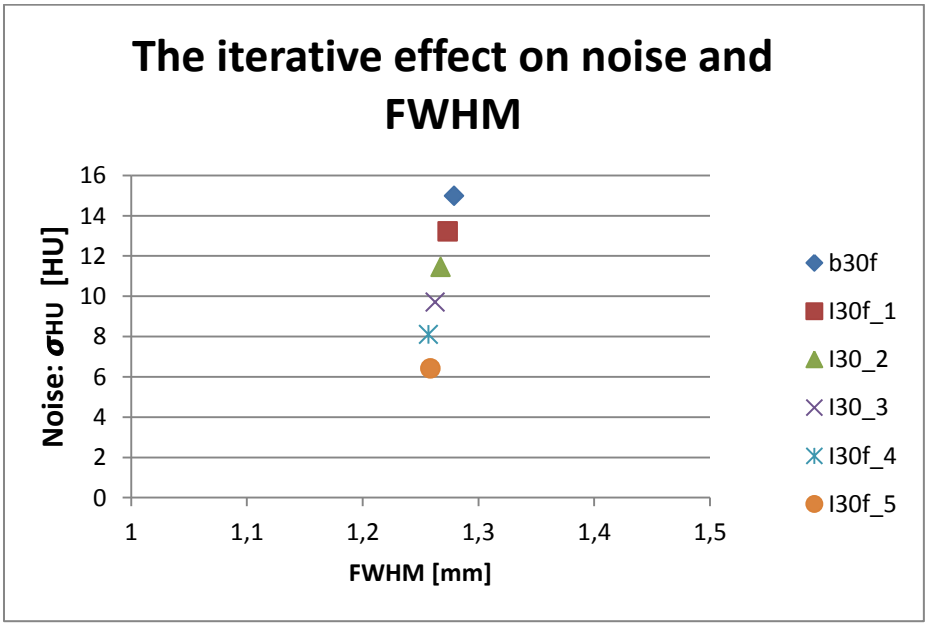

Figure 44: The graph shows noise as a function of FWHM and iterative level. The information is collected from images of the Catphan phantom taken at 200 mAs. The noise is reduced when increasing the number of iterations. There is no significant change in FWHM when increasing the number of iterations.

4.1.2 *The effect on the Noise Power Spectrum*

The area under the NPS curves, the noise, decrease as expected as a function of mAs (See Figure 45). The curves have similar shapes, and by calculating a weighted mean value all the curves show a mean spatial frequency of 3,0 lp/cm (line pairs per cm).

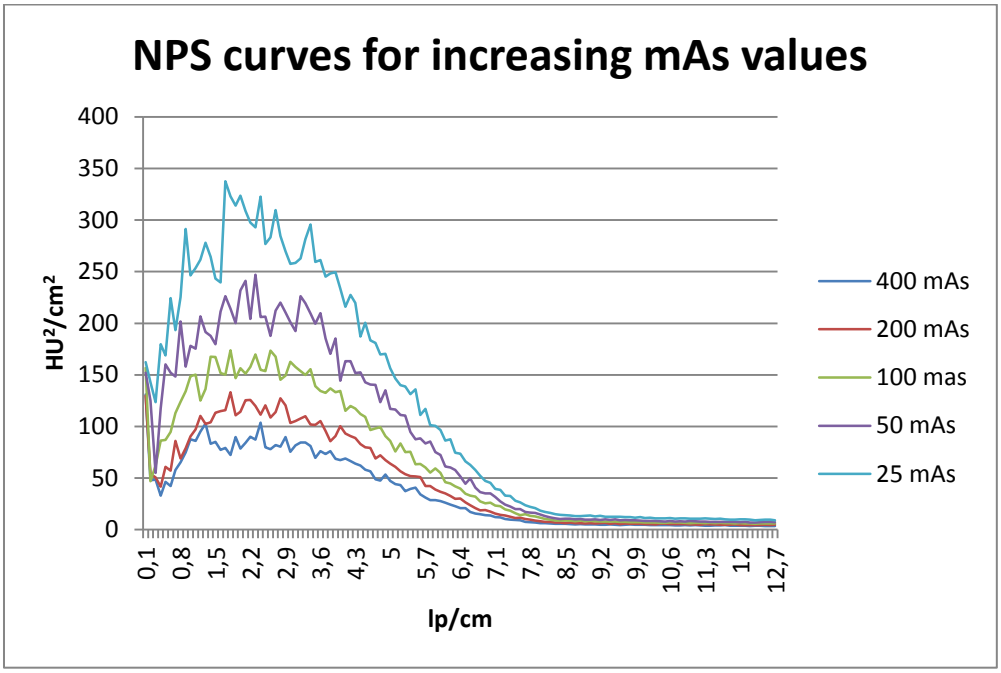

Figure 45: NPS curves for increasing mAs values, taken with a soft filter B30, filtered back projection.

The noise also decreases as a function of increasing iterative level. However, as the iterative level increases the curves has a minor shifted towards lower spatial frequencies. This minor shift was found for all filters explored in this study, i.e. filters 30, 31, 40, 41 and 70. The weighted mean spatial frequency for the B30 filter is 3,0 lp/cm, while it is 2,75 lp/cm for the I30_5 setting. This shift to the left with increasing iterative level may reflect the blotchy appearance experienced by radiologist when using a high iterative level (see Figure 46).

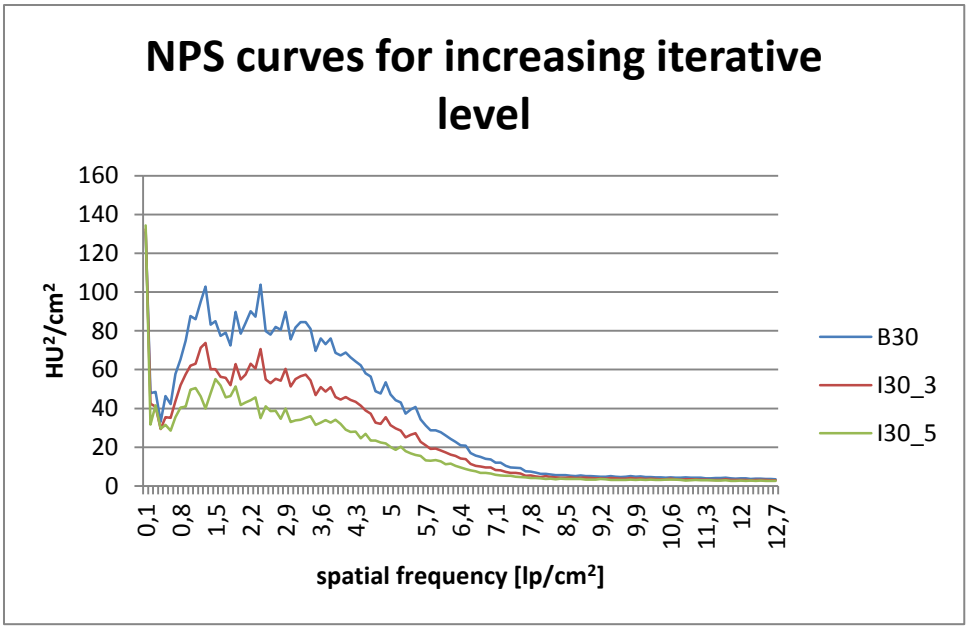

Figure 46: NPS curves for noise images taken at 400 mAs with a soft filter 30, with increasing iterative level.

The shift occurring when using a sharper filter is quite visible as seen in Figure 47 and the weighted mean spatial frequency increases from 3,0 lp/cm to 3,75 lp/cm, an increase of 25%, when changing the filter from B30 to B41.

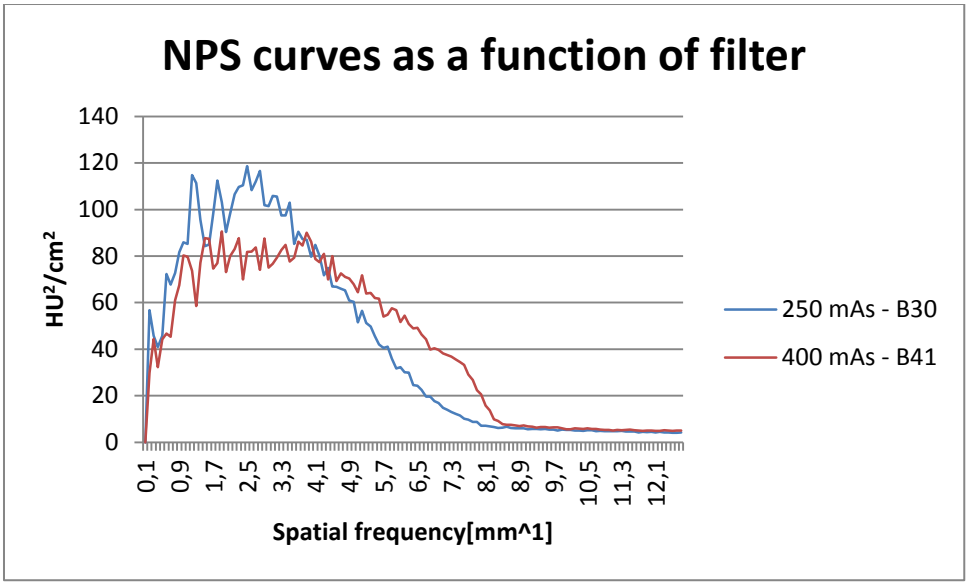

Figure 47: NPS curves for two different filters, a softer filter 30 and a sharper filter 41. The mAs has been reduced for the B30 filter to obtain same noise level as the B41 filter (σ_{HU} = 13 HU). This mAs difference has no influence on the distribution or the weighted spatial frequency as shown in figure 37.

The noise level, defined as the standard deviation in HU values (σ_{HU}), for the two settings illustrated in Figure 47 is the same. However, as the distribution of the noise is different, one of the settings (in this case 250 mAs – B30) will appear noisier, as the noise is coarser (see Figure 48).

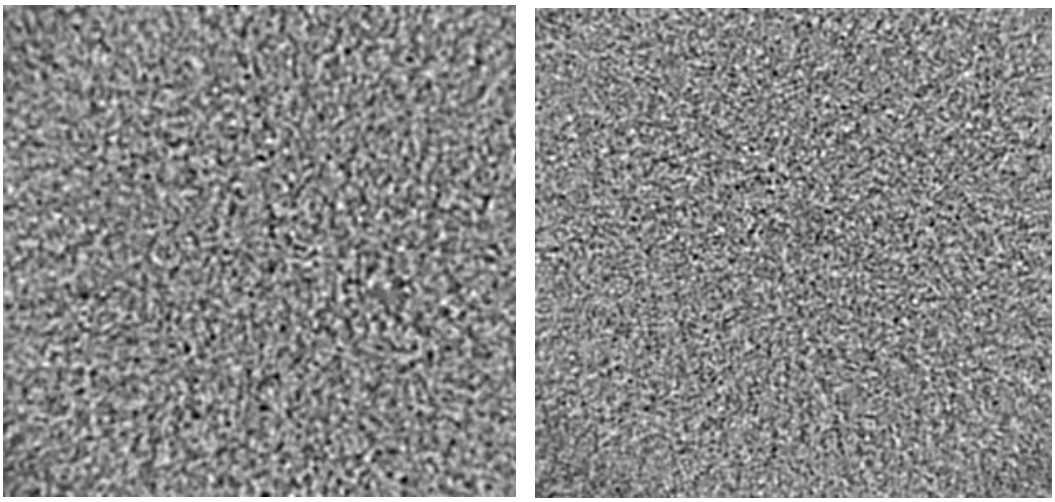

Figure 48: Images from the homogeneous region of the Catphan phantom taken at 250 mAs reconstructed with B30 (to the left) and 400 mAs reconstructed with B41 (to the right). The standard deviation in HU values (σ_{HU}) is 13 for both images.

4.1.3 ALTERNATIVE LOWER DOSE SETTINGS FOR THE ABDOMEN AREA

Initially three different sharper filters where considered as alternatives to the nominal filter, 30, for abdomen. However, as the 40 filter showed no improvement in FWHM, while an increase in noise (see Figure 42), this option was left out. In addition, the gastro radiologist claimed the 41 filter to be too edge-enhancing to be used in the abdomen, leaving filter 30 and 31 to be further investigated.

For filter 30 and 31 some initial eliminations on iterative strength where made based on the results from Figure 43. The lower dose alternatives for abdomen with their resulting FWHM and noise values can be seen in Figure 49 and Figure 50.

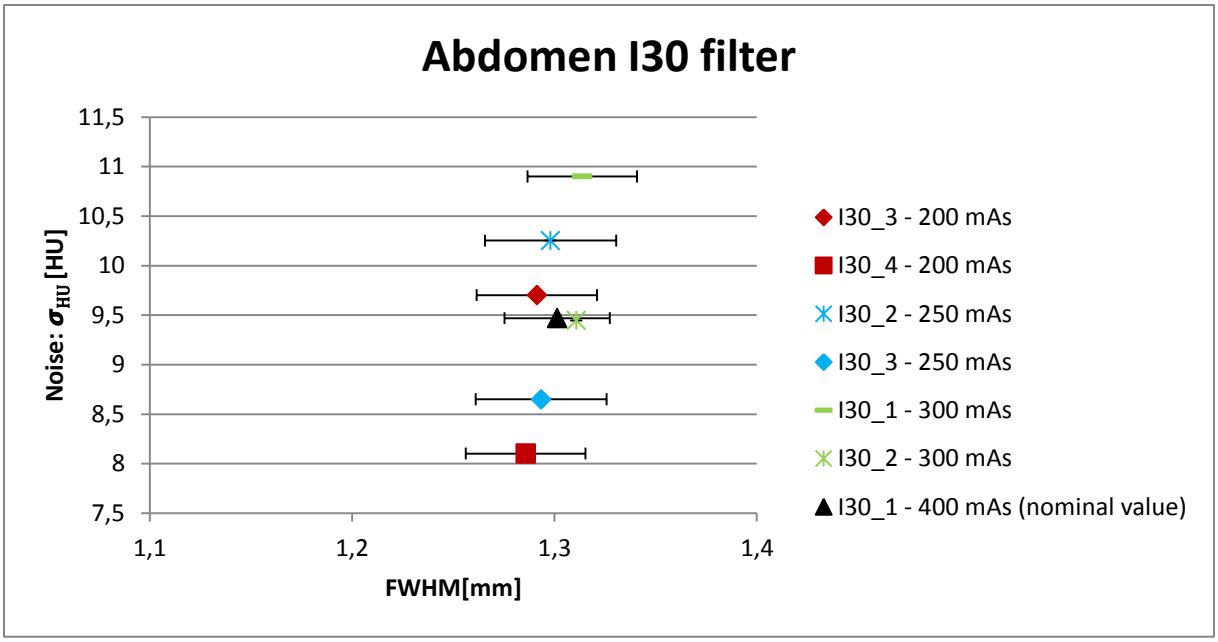

Figure 49: The graph shows the noise level and FWHM for all the lower dose alternative settings together for filter 30 with the reference setting for the abdomen area. Red markers represent 50% dose level, blue markers 62,5% dose level and green markers 75% dose level. The black marker is the reference value at 400 mAs. Error bars based on STD of 10 repetitive scans (standard deviation of 2,0 – 3,5 %) has been plotted. The noise had negligible uncertainty with a STD of approximately 0,4%.

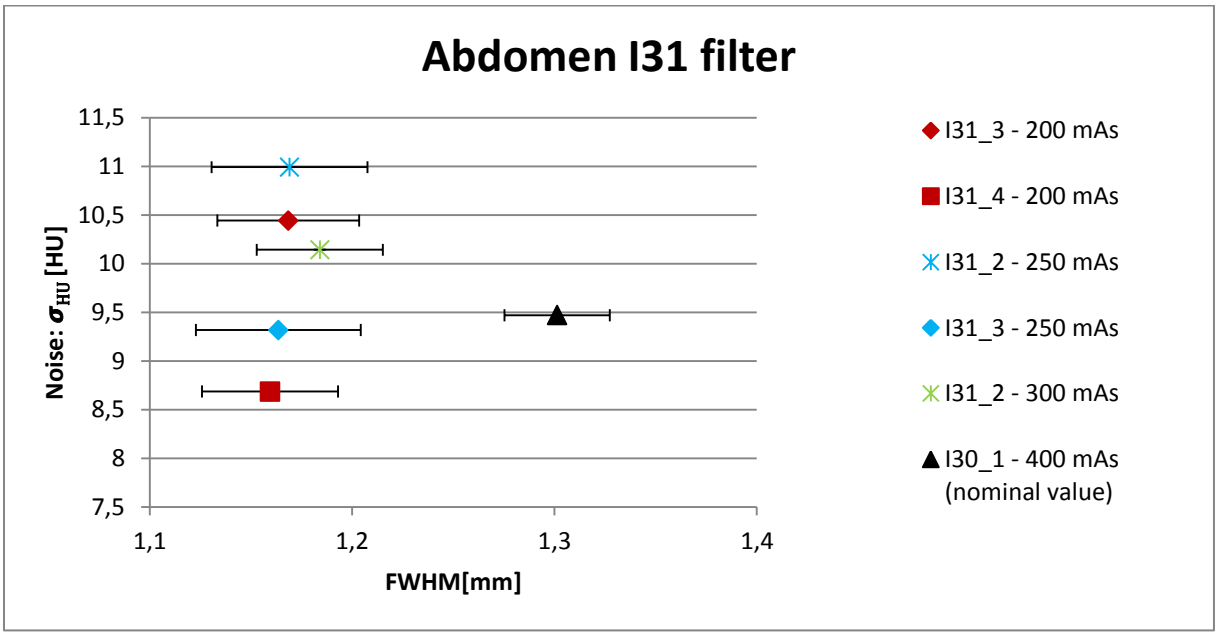

Figure 50: The graph shows the noise level and FWHM for all the lower dose alternative settings together for filter 31 with the reference setting for the abdomen area. Red markers represent 50% dose level, blue markers 62,5% dose level and green markers 75% dose level. The black marker is the reference value at 400 mAs. Error bars (standard deviation of 2,0 – 3,5 %) has been inserted The noise had negligible uncertainty with a STD of approximately 0,4%.

As expected, applying filter 31 versus 30, gives an improvement in FWHM with an increased noise level (see Figure 50). However, for the 31-alternatives chosen, the noise is at the same level as the noise at the nominal setting.

The uncertainty for all the measured FWHM values were 2 – 3,5 %. The noise had negligible uncertainty with a STD of 0,4 %.

The results on which alternatives fulfills the criteria can be seen in Table 4.

Table 4: The possible alternatives fulfilling the noise and FWHM criteria.

Dose level	Parameter settings fulfilling noise and FWHM criteria
50 % (200 mAs)	I30_4, I31_4
62,5% (250 mAs)	I30_3, I31_3
75% (300 mAs)	I30_2

4.1.4 ALTERNATIVE LOWER DOSE SETTINGS FOR MEDIASTINUM

The assumptions for lower dose alternatives made for the mediastinum can be seen in Figure 51 and Figure 52. The nominal parameter setting for mediastinum, 40 mAs and reconstruction I31_3, had a standard deviation of 5,2% on the FWHM values. For the lower dose alternatives the STD varied between 4,3 % and 11 %. Due to the high STD, all the lower dose alternatives have average FWHM values within 1 STD of the reference values, indicating no significant improvement of FWHM when applying the sharper filter 41. However, the noise is generally higher for the 41 filter.

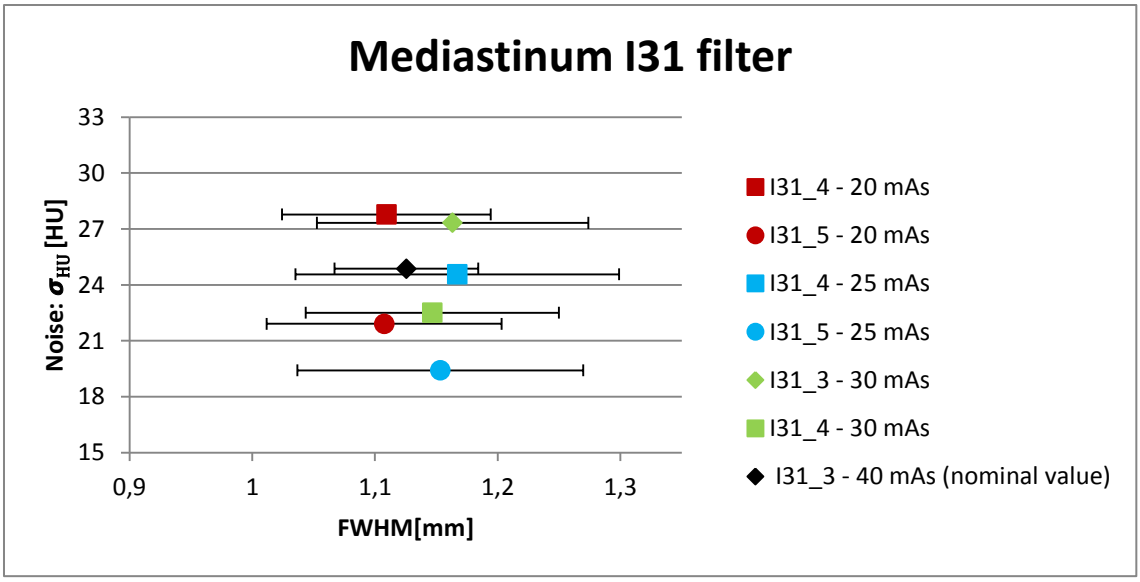

Figure 51: The diagram shows the lower dose alternatives with filter 31 for the mediastinum nominal setting at 40 mAs, with error bars. Red markers represent 50% dose level, blue marks 62,5% dose level and green markers 75% dose level. The black mark is the reference value at 40 mAs (100% dose).

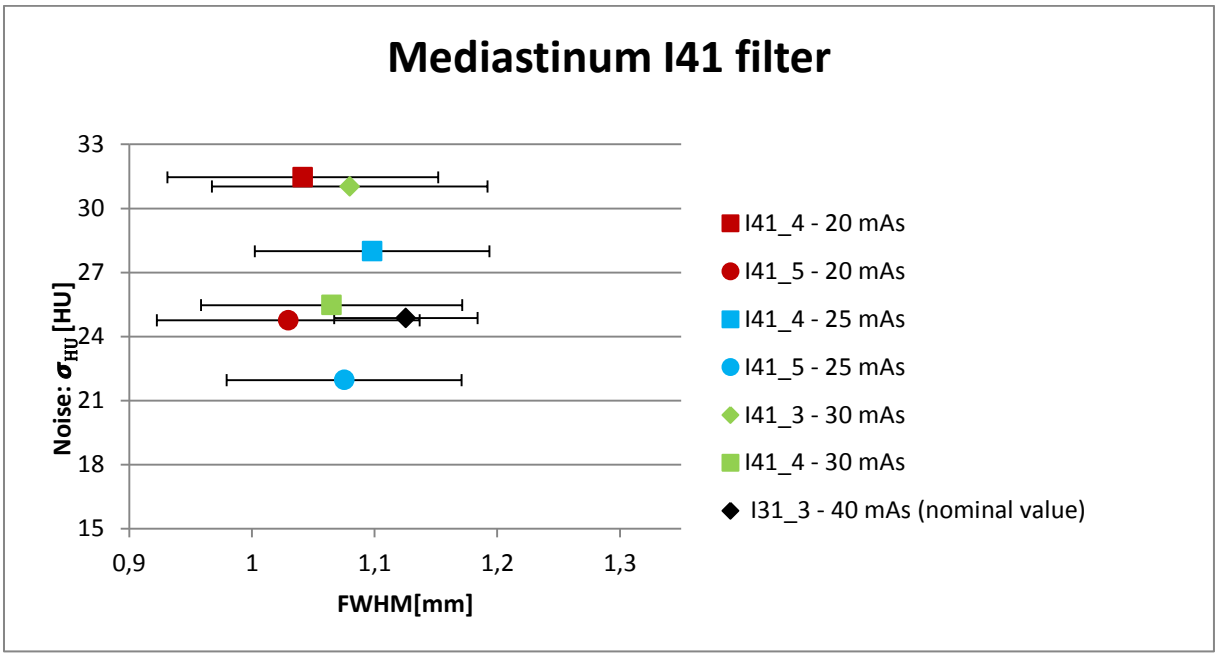

Figure 52: The diagram shows the lower dose alternatives with filter 41 for the mediastinum reference setting at 40 mAs, with error bars. Red markers represent 50% dose level, blue marks 62,5% dose level and green dots 75% dose level. The black mark is the nominal value at 40 mAs (100% dose).

The results fulfilling the noise and spatial resolution criteria for mediastinum can be seen in Table 5.

Table 5: The lower dose alternatives fulfilling the criteria set initially.

Dose level	Settings fulfilling noise and FWHM criteria
50 % (20 mAs)	I31_5, I41_5
62,5% (25 mAs)	I31_4, I31_5, I41_5
75% (30 mAs)	I31_4

4.1.5 ALTERNATIVE LOWER DOSE SETTINGS FOR LUNGS

For the lung area, only filter 70 was explored when examining the use of iterative strength. The STD's for the FWHM values were relatively high, varying between 4-8 % (see Figure 53).

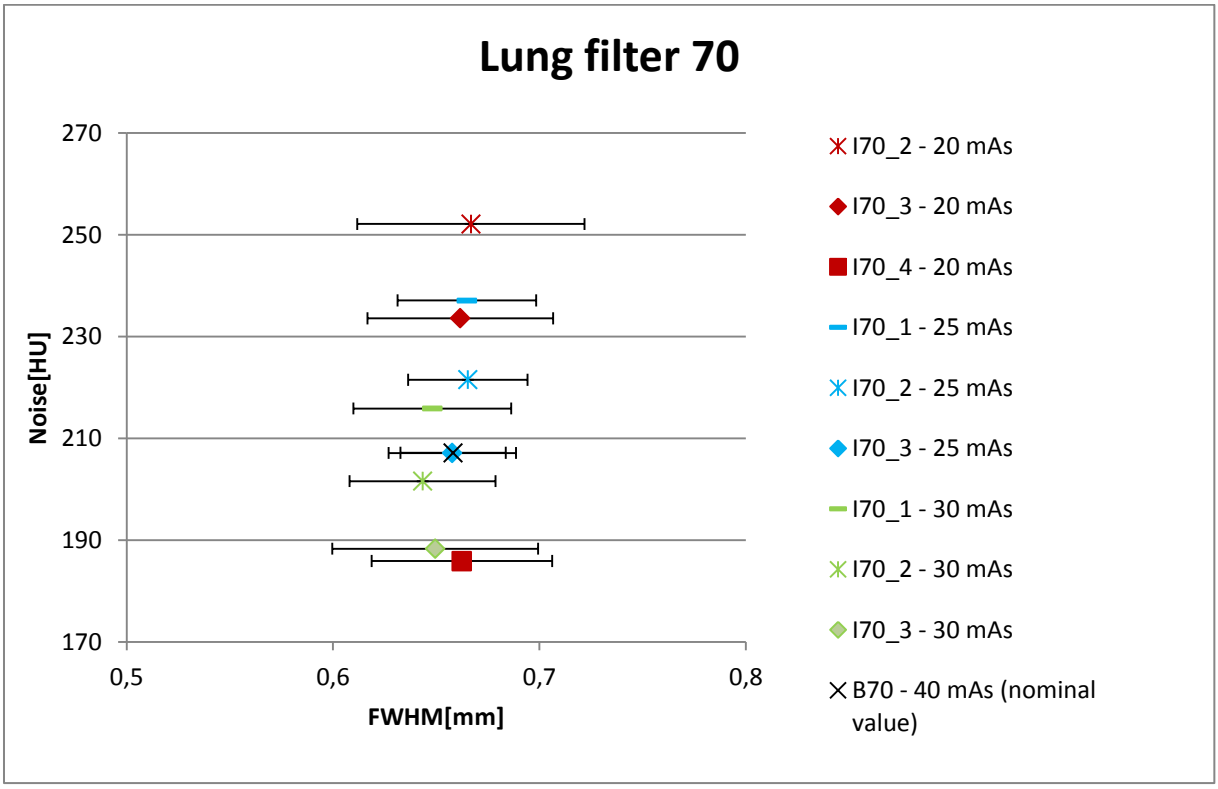

Figure 53: The graph shows the FWHM and noise values for given lower dose alternatives together with the reference values for the lung protocol, 40 mAs and a B70 filter. There is no significant change in FWHM for the different lower dose alternatives.

Table 6: The lower dose alternatives fulfilling the image quality criteria.

Dose level	Settings fulfilling noise and FWHM criteria
50 % (20 mAs)	I70_4
62,5% (25 mAs)	I70_3
75% (30 mAs)	I70_2, I70_3

When analyzing the noise characteristics for the 70 filter at 50 % dose level alternative, doing a large leap from a nominal filter setting without any iterations (FBP) to an iterative level of 4, the minor shift found in Figure 46 with increasing iterative level, gets more visible, as shown in Figure 54 and visualized in Figure 55. The noise level for B70 at the nominal dose (40 mAs) is the same as the noise level at 20 mAs using iterative level of 4. However, the NPS curve for the lower dose alternative is slightly shifted towards lower spatial frequencies, from a weighted mean spatial frequency of 5,35 lp/cm to 5,09 lp/cm.

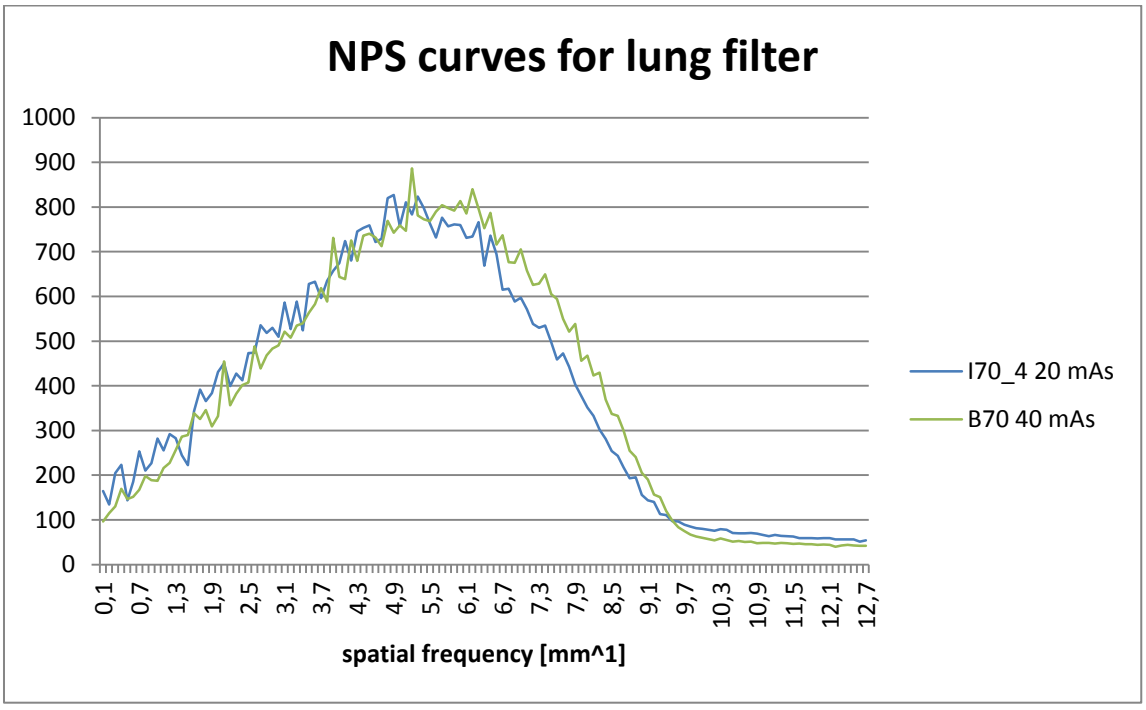

Figure 54: NPS curves for a 50 % dose reduction alternative for the lungs.

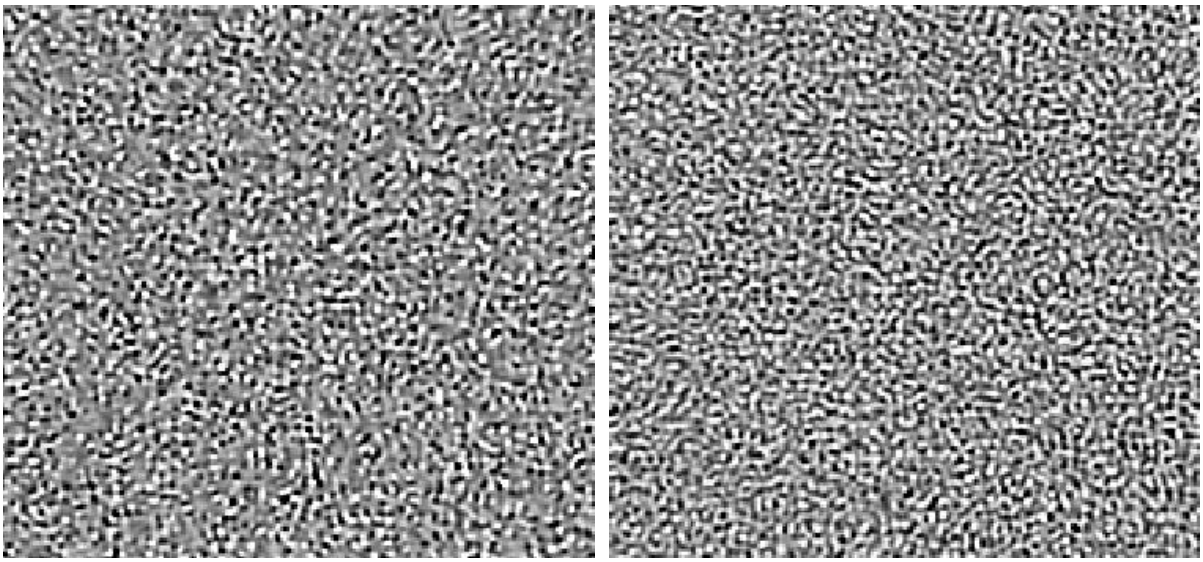

Figure 55: To the left: Noise image taken at 20 mAs reconstructed with I70_4. To the right: noise image taken at 40 mAs, reconstructed with B70 (FBP). The noise distribution is slightly coarser and appears "patched" in some regions for the noise image taken with a high iterative strength shown to the left.

Based on the knowledge of blotchy appearance experienced by radiologists at the high iterative level 4 and 5, it was an aim to keep the iterative level as low as possible without compromising on noise level. However, for some of the alternatives at 50% dose level and 62,5% level this was not possible due to the image noise criteria. As a result, some more alternatives where eliminated,, leaving the alternatives shown in Table 7 to be examined further using the anthropomorphic phantom.

Table 7: The table shows the lower dose alternatives chosen which fulfills the criteria of maintained/improved noise level and maintained spatial resolution. These alternatives where applied on the anthropomorphic phantom.

Anatomic area	Alternative 1 (50% dose)	Alternative 2 (62,5%dose)	Alternative 3 (75% dose)	Nominal settings (100% dose)
Mediastinum	I31_5 I41_5	I31_4 I41_5	I31_4	I31_3 - 40 mAs
Lungs	I70_4	I70_3	I70_2	B70 – 40 mAs
Abdomen	I30_4 I31_4	I30_3 I31_3	I30_2	I30_1 – 400 mAs
quality reference mAs	120 ref. qual. mAs	150 ref. qual. mAs	180 ref. qual. mAs	240 ref. qual. mAs

4.2 OBJECTIVE ANALYSIS OF ANTHROPOMORPHIC PHANTOM

4.2.1 THE ABDOMEN AREA

When comparing the signal-to-noise and contrast-to-noise ratio calculated on all low dose scans to the SNR and CNR on the nominal reference scan, all the lower dose alternatives showed improved SNR and CNR, compared to the reference dose at 240 mAs (see Figure 56). SNR and CNR at 50% dose reduction with the same parameter settings as the reference settings has also been included to better illustrate how SNR and CNR are significantly decreased when only reducing the dose and not increasing the iterative level.

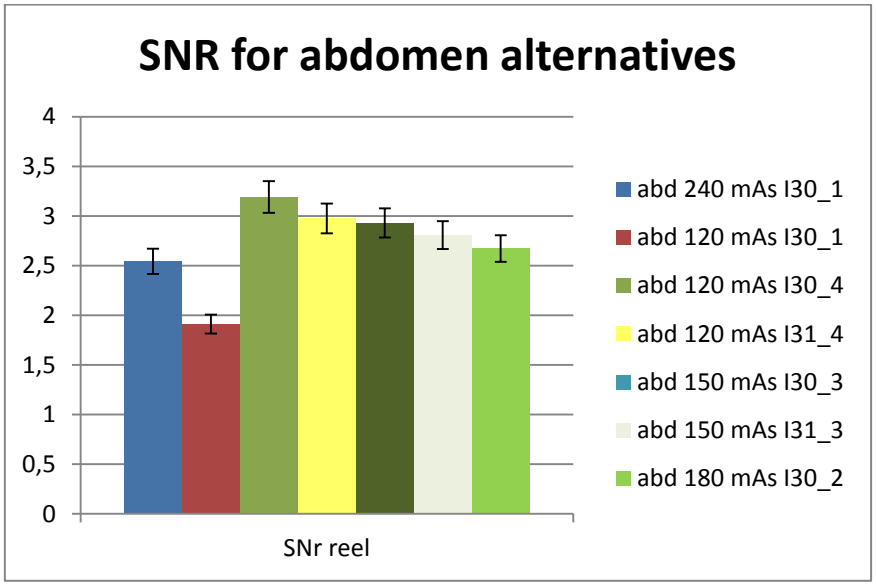

Figure 56: The graph shows the SNR for ROI1 in the lever. The blue column shows the SNR for the nominal parameter settings with 100% dose. The red column shows the SNR for the nominal parameter settings with 50% dose. The other columns show the SNR for different dose level, filters and iterative level. Error bars of 5% has been added. This is an estimated error, based on the maximum of the standard deviations for the different alternatives.

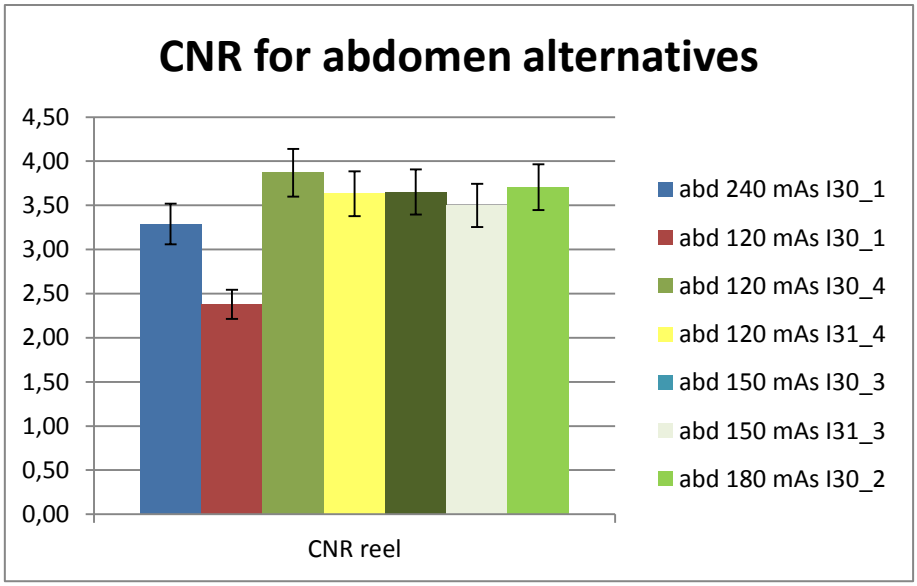

Figure 57: The graph shows the CNR ROI1 placed in the liver and ROI2 placed outside the liver. The blue column shows the SNR for the nominal parameter settings with 100% dose. The red column shows the SNR for the nominal parameter settings with 50% dose. The other columns show the SNR for different dose level, filters and iterative level

The error bars is based on an estimate. As only two scans of the anthropomorphic phantom were performed, it gives a poor foundation of standard deviations. However, calculations were yet performed and an average of these uncertainties found, weighing the highest uncertainties more, was used for all alternatives.

4.2.2 FOR THE MEDIASTINUM

For the mediastinum SNR and CNR was highest for the reference setting (100% dose, quality reference mAs of 240, filter I31_3), but not significantly higher than the lower dose alternatives. One exception was found at 50% reduction (quality reference mAs of 120) with filter I41_5, which showed same SNR and CNR level as the 50% reduction without altering the filter (the red graph). See Figure 58.

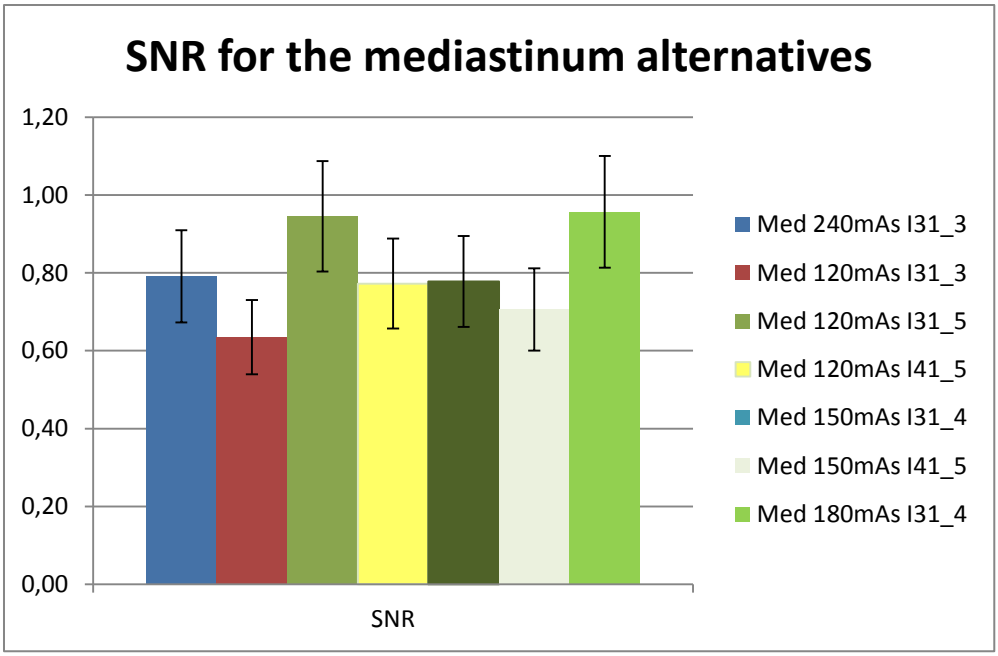

Figure 58: There was no significant reduction in SNR for the lower dose alternatives shown in this diagram. However, due to high uncertainty even the 50% dose reduction alternative with same filter/iteration strength as the reference protocol at 100% does not appear to have a significantly lower SNR.

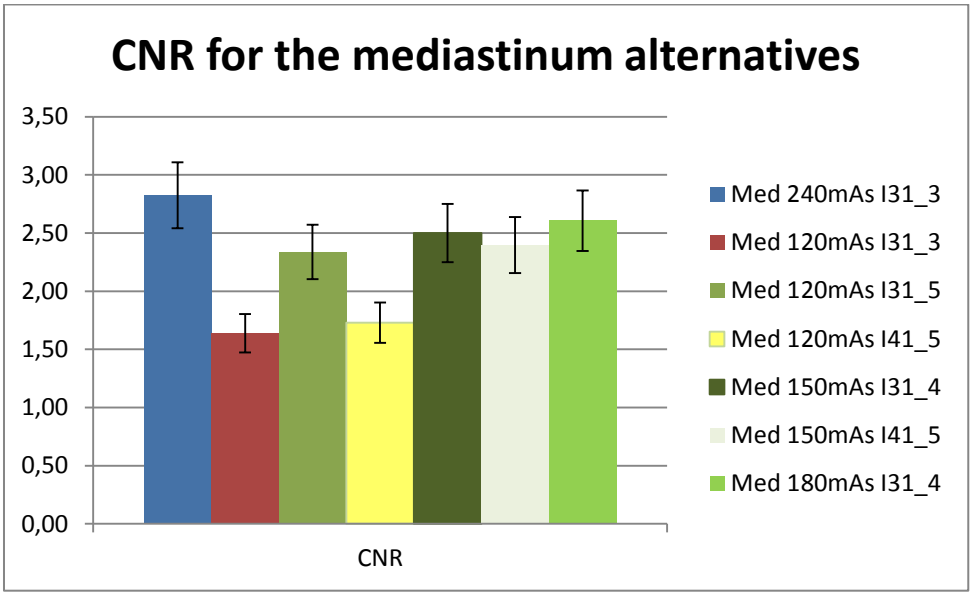

Figure 59: The graph shows the CNR between the the lymph node (ROI2) and inter-mediastinal tissue (ROI1). There was no significant reduction in CNR, except for the 50% dose reduction using alternative filter I41_5.

4.2.3 FOR THE LUNGS

As the lungs in the anthropomorphic phantom were missing lung tissue (See Figure 40), a subjective examination of image quality of the scans of the anthropomorphic phantom analyzed by the thorax-radiologist had to be excluded.

Based on the results obtained from the Catphan analysis, and the SNR and CNR analysis from the anthropomorphic phantom following alternatives where analyzed by the radiologists:

Table 8: The lower dose scan parameter settings applied on scans of the anthropomorphic phantoms and sent to the radiologists for evaluation.

Anatomic area	Reference settings (100% dose)	Alternative 1 (50% dose)	Alternative 2 (62,5%dose)	Alternative 3 (75% dose)
Mediastinum	I31_3 - 40 mAs	I31_5	I31_4	I31_4
Lungs	B70 – 40 mAs	I70_4	I70_3	I70_2
Abdomen	I30_1 – 400 mAs	I31_4	I31_3	I30_2
all	240 ref. qual. mAs	120 ref. qual. mAs	150 ref. qual. mAs	180 ref. mAs

For abdomen there was no significant difference in SNR and CNR between the various lower dose alternatives. However, based on the knowledge of the NPS curves and the finer graininess appearing for the sharper filter 31 compared to 30, the 31 filter was chosen as best alternative at 50% and 62,5% dose level.

4.3 SUBJECTIVE ANALYSIS OF ANTHROPOMORPHIC PHANTOM

4.3.1 ABDOMEN

The four alternatives represented for the gastro-radiologist:

Filter	Dose level	Quality reference mAs
I30_1 (nominal setting)	100%	240 mAs
I30_4	50%	120 mAs
I30_3	62,5%	150 mAs
I30_2	75%	180 mAs

Out of the three lower dose alternatives, the lower dose alternative at 75% of original dose level, using filter I30_3 was considered to have approximately same image quality as the nominal setting at 100% dose level. In general, noise was not a problem. However, he experienced small organs with small differences in contrast and small space between them like aorta and surrounding tissue being more difficult to separate at the 62,5 % and 50% alternatives.

4.3.2 MEDIASTINUM

For the lower dose alternatives presented for the thorax radiologist, all the lower dose alternatives was stated as having good enough image quality. However, this statement is based on the few structures available in the phantom. As already mentioned, the phantom is lacking several important structures in this anatomic area.

5 DISCUSSION

THE OBJECTIVE EVALUATION USING CATPHAN

For the abdomen area, with nominal exposure value of 400 mAs and filter B30, iterative strength 3 was needed to be able to reduce the dose with 50 % while maintaining the same noise level. This is in line with literature studying objective image quality (von Falck, Bratanova et al. 2013) where I30_3 at 100 mAs reached the low-contrast performance of dataset reconstructed with FPB, B30, at 200 mAs. Also studies performed on patients (Winklehner, Karlo et al. 2011) show similar image quality using iterative strength 3 combined with 50% dose reduction.

For mediastinum, which already had an iterative level of 3, two levels up in iterative strength gave the same noise level as the nominal scan parameters, while for the lungs with a reference setting using only FBP, 4 iterative levels was needed to maintain the same noise level at 50% dose level. For the 62,5% and 75% dose level, lower iterative strengths were needed to maintain the same noise level as for 100% dose level.

When considering the filters 31 and 40 as an alternative for filter 30 for the abdomen, no significant difference in FWHM was found, only an increase in noise for filter 40. Due to this apparent insignificant improvement in FWHM (while an increase in noise), filter alternative B40 was left out.

According to Siemens (Siemens 2007) filter 30 and 31 has same spatial resolution and 40 and 41 has the same spatial resolution. According to Siemens the filters 31 and 41 only have a different noise distribution compared to filter 30 and 40, respectively. However, this is not in line with the results obtained from the objective measurements of FWHM, where there was an significant increase in spatial resolution when going from filter 30 to 31, and also an increase going from 40 to 41.

The NPS curves show a small shift to the left when increasing the iterative level, meaning coarser graininess in the noise. This is consistent with literature stating that especially iterative level of 4 and 5 gives the images somewhat blotchy appearance (Yang, Yan et al. 2013).

Due to the visual perception of blotchiness with increasing iterative level, the vendors normally do not recommend using the two highest levels of iterations (Andreassen

2013). This generated a problem when trying to find a lower dose alternative for the mediastinum protocol, as this reconstruction volume already contains an iterative level of three.

5.1.1 UNCERTAINTY

The uncertainty (standard deviation) for the measured noise at all relevant mAs values and filters where found to vary between 0,4% and 1,1% and has therefore been left out in the diagrams due to the fact that the error bars where shorter/smaller than the colored markers themselves.

For the FWHM value the uncertainty was typically between 0,5 and 11% The uncertainty was highest for the images taken at the lowest mAs values (20 mAs – 40 mA) which were the values examined for mediastinum and lungs. The standard deviation of the FWHM values at these mAs values varied between 4,4 % up to 11 % at these low mAs values.

When running the PSF_noise program 10 times for the exact same image of the bead, and doing an uncertainty analysis, the standard deviation of the FWHM values was found to be 0,2% and therefore do not contribute with any significant error to the total standard deviation for the FWHM. Nevertheless, when analyzing 10 different images of the bead in the PSF_Noise program, all taken at with same mAs and reconstruction filter, this error is automatically included.

The main source of error in the PSF_Noise program is the assumption on Gaussian distribution of the PSF. At low exposure (20 mAs – 40 mAs) there is less information (less radiation hit the detector) available to form this curve and higher uncertainty in the shape of the curve. As seen in Figure 60, the approximation of a Gaussian distribution of the PSF_Noise curve less valid at the lower exposures.

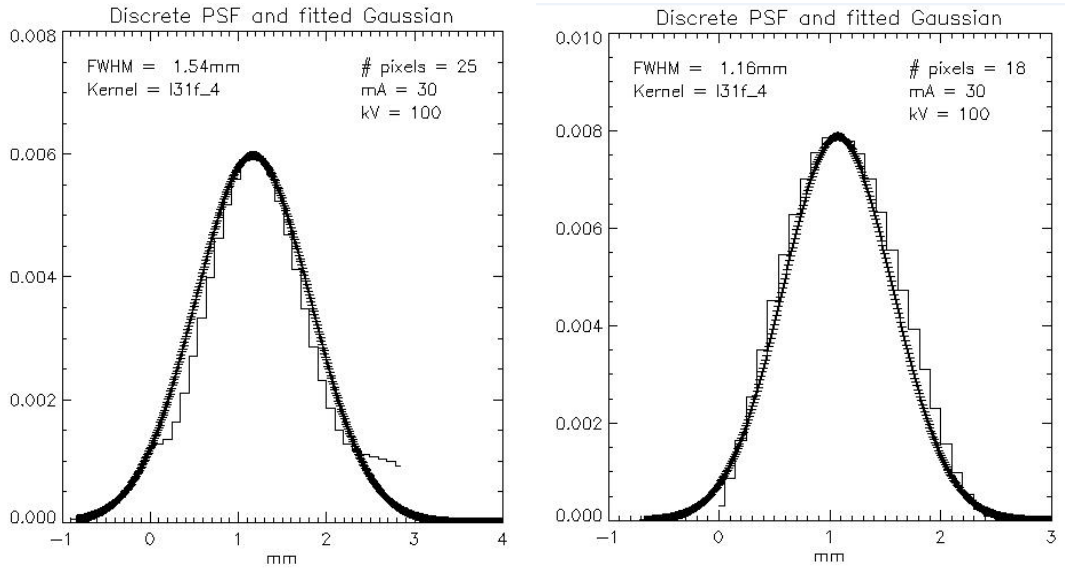

Figure 60: The figure shows two different PSF taken at 25 mAs with filter I31_4. The Gaussian fit is placed outside the pixel values in the image to the left, probably due to the "tail" seen in lower right corner. The calculated FWHM value for the curve to the left is 33% higher.

The Gaussian approximation was even poorer for the sharp 70 filter. Using the sharp lung filter at low mAs values, the bead was reproduced over only a few (6-7) pixels compared to the softer filter where the bead is smeared over approximately 20 pixels. This was somewhat corrected for by cutting the results giving aberrant FWHM values, like depicted in Figure 61 where some pixel values apparently are not registered in the PSF_Noise program resulting in a poor fitted Gaussian.

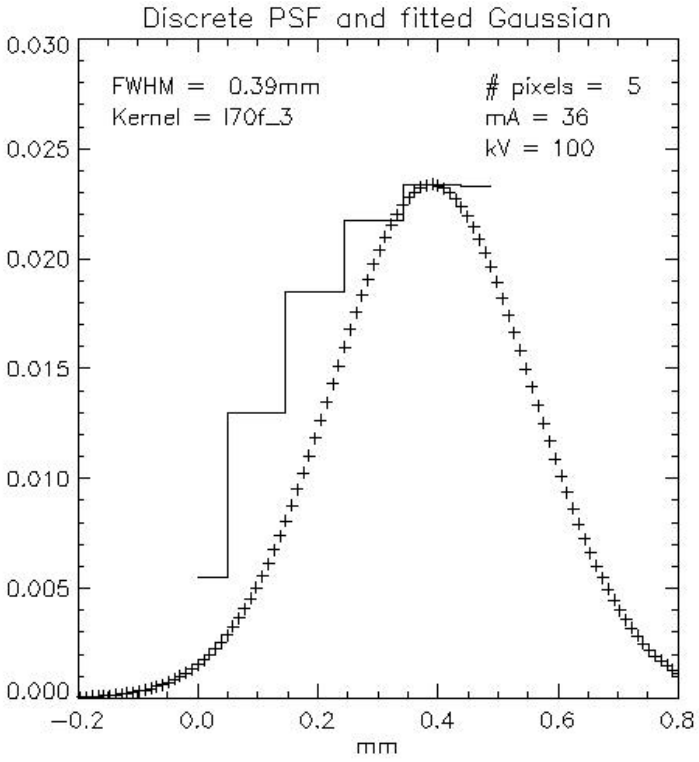

Figure 61: An aberrant result for the FWHM values taken with the sharp 70 filter at low mAs value.

Due to the high uncertainty at the low exposure values (20 mAs – 40 mAs) no significant improvement when using sharper filter could be verified.

5.2 OBJECTIVE EVALUATION OF THE ANTHROPOMORPHIC PHANTOM

The SNR and CNR values were based on the average obtained from to separate scans. More scans should have been done to give a better estimate and obtain lower uncertainty. With the high uncertainty estimated from the two scans, SNR for 50% dose reduction for mediastinum while keeping the same filter as 100% dose, show no significant reduction in SNR. From theory (Curry, Dowdey et al. 1990) SNR is known to decrease with decreasing mAs if no other parameters are changed. The high uncertainty in the measured values may have led to the false conclusion to exclude reconstruction alternative I41_5 at 50% dose level. Based on the noise results from the Catphan analysis using PSF_noise this reconstruction alternative should have maintained same CNR and SNR level as the other alternatives. Lastly, there is a potential risk of falsely getting the result SNR = 0 when using this method, using CT numbers in the calculations instead of attenuation numbers, if e.g. calculating SNR in water.

As for the liver in the abdomen, the CNR between the liver and the vessels embedded would have been a better measurement on the low-contrast detectability as their visibility is one of the image quality criteria used by the radiologist. However, this was difficult to implement with the homemade Python program used. Low-contrast visibility is as mentioned in section 2.5 not only dependent on contrast and noise, but also on the diameter of the low contrast detail. As the ROI's used in the CNR calculations in this study are of rather large sizes, this aspect of low contrast detectability is not implemented. In an extension of this work, calculations of CNR with circular ROI's in the low-contrast circles in the Catphan phantom might give better results as these circles have decreasing diameter and known nominal contrast.

In general, the calculation of SNR and CNR is rather simple measurements of image quality (von Falck, Bratanova et al. 2013; Wang, Schoepf et al. 2013). It also does not always correlate well with the judgment of human readers (von Falck, Bratanova et al. 2013), which in the end must be considered the gold standard. However, SNR and CNR still give an objective analysis of image quality as it gives information on image information versus noise, the latter known to strongly influence the human reader's perception of image quality. It is also much less time consuming than using human readers.

5.3 SUBJECTIVE EVALUATION OF THE ANTHROPOMORPHIC PHANTOM

The image quality of the anthropomorphic phantom was only evaluated by one radiologist for each anatomic area, making the result highly subjective and individual giving that all radiologists has a different perspective on image quality. To fully obtain a sufficient image quality analysis several human observers should participate, using visual grading techniques such as visual grading analysis (VGA) where a point scale is used to grade the image qualities or image criteria (IC) before an IC-score is calculated based on the ratios of fulfilled criteria (Ludewig, Richter et al. 2010). The radiologist evaluating the image quality in abdomen based his decisions purely on how visible he perceived the low-contrast details in the lever compared to the reference image, the shape of the liver edge, the edge of the pancreas and general sharp visualization of the other organs in the anthropomorphic phantom. Ideally, lesion detectability should have been evaluated as lesion detectability is the main purpose of diagnostic imaging.

Therefore are several general challenges connected to this subjective evaluation method when there are no lesions present. Identifying the radiation dose at which lesions become undetectable, delineating the difference between maintained image quality in the form of noise level and spatial resolution and maintained diagnostic performance are two issues which becomes impossible to solve without any lesions present in the anthropomorphic phantom.

Another problem was raised when the radiologist evaluating the thorax area found the lungs in the anthropomorphic phantom to be missing lung tissue. Only the main lung artery was seen in the thorax, making it hard to make any conclusions for this area based on the anthropomorphic phantom.

5.4 OBJECTIVE IMAGE QUALITY VERSUS SUBJECTIVE IMAGE QUALITY

The link between objective image quality parameters and the visual perception of the readers is hard to find. By merely doing an objective approach, the dose generally can be reduced minimum 50 % without reducing physical image quality parameters such as noise, spatial resolution, SNR and CNR and virtual lesion detectability (Kalra, Maher et al. 2003; von Falck, Bratanova et al. 2013).

The CT scans sent to the gastro radiologist for evaluation of image quality all contained lower/equal noise level and improved/maintained spatial resolution in addition to improved/maintained CNR and SNR. Nevertheless, only the lower dose alternative closest to the nominal setting was considered being of similar image quality as the nominal setting. Many radiologists seem to dislike the unfamiliar look images reconstructed with iterative techniques get (Singh, Kalra et al. 2012; Yang, Yan et al. 2013). However, it can be discussed whether this blotchy appearance experienced by the radiologists affects the diagnostic detectability of lesions.

A prospective study performed by Singh *et al* evaluated 22 patients using iterative reconstruction techniques combined with up to 75% dose reduction (Singh, Kalra et al. 2010) found that no lesions were missed when combining iterative techniques and dose reduction compared to FBP (100% dose) which may indicate that although the images gets blotchier, it do not affect the lesion detectability. On the other hand, in a study

performed by Fletcher et al using SAFIRE at 50% dose level compared to 100% dose the diagnostic confidence showed to vary within the reader-group (Fletcher, Krueger et al. 2013). This demonstrates the importance of close dialog with the radiologists when optimizing protocols with dose reduction. Although there is a foundation from literature to reduce the dose using iterative techniques, the local radiologists' evaluation must still be considered as the golden standard.

To finalize the optimization process of the thorax-abdomen/pelvis protocol investigated in this study, several patient scans with the lower dose alternatives should be performed and evaluated by experienced radiologists. The most promising alternative is the 75% dose level with quality reference mAs of 180, using filter I30_2 for the abdomen area as this was the only lower dose alternative being accepted by the gastro radiologist. The filter and iterative level used for mediastinum does not need to be changed at 25 % dose reduction. The nominal parameter setting already uses an iterative level of 3, and while increasing the iterative level reduces the noise, the blotchy appearance seen in patients scans using a high iterative strength(Yang, Yan et al. 2013), gives an undesirable and unfamiliar "look" in the images. The reason for allowing more noise in the mediastinum area is that the standard protocol for the thorax area (only thorax, not thorax-abdomen/pelvis) has a much lower reference mAs than the combined protocol investigated in this study. The combined thorax-abdomen/pelvis protocol has quality reference mAs of 240 which is also the same for the abdomen protocol, compared to normally a quality reference mAs of 110 for the thorax protocol.

Based on this difference in quality reference mAs for a typical thorax protocol and a typical abdomen protocol there might be a potential for even further dose savings by splitting this combined protocol into two separate scans, one for abdomen/pelvis and one for thorax, with different quality reference mAs for the two protocols.

Ideally, further dose levels of 50% and 62,5 % should have been investigated on patient scans in order to be able to analyze the difference in image quality and try to connect the results obtained from the objective image quality analysis with human observers. However, without any profound evidence that the image quality would be adequate at these large reductions it would require approval from ethical committee and patients competent to give informed consents.

6 CONCLUSIONS

Analyzing images of the Catphan 600 phantom by measuring PSF_NOISE and NPS curves is easy to perform and interpret, and is therefore an effective way of eliminating irrelevant scan parameters in order to narrow down the options used for further investigation. The objective image quality analysis using Catphan 600 phantom and an anthropomorphic phantom yielded a dose saving potential of 50%. However, this did not fully reflect the subjective image quality perception of the experienced radiologists. A potential dose reduction of 25% of the current thorax-abdomen/pelvis scan protocol is clinically feasible.

7 REFERENCES

Andreassen, H. (2013). Applicatient Specialist, Siemens.

Baker, M. E., F. Dong, et al. (2012). "Contrast-to-noise ratio and low-contrast object resolution on full- and low-dose MDCT: SAFIRE versus filtered back projection in a low-contrast object phantom and in the liver." AJR Am J Roentgenol **199**(1): 8-18.

Bakke, K. A. (2011) "The Use of CT is Doubled."

Baumueller, S., A. Winklehner, et al. (2012). "Low-dose CT of the lung: potential value of iterative reconstructions." Eur Radiol **22**(12): 2597-2606.

Beister, M., D. Kolditz, et al. (2012). "Iterative reconstruction methods in X-ray CT." Phys Med **28**(2): 94-108.

Boedeker, K. L., V. N. Cooper, et al. (2007). "Application of the noise power spectrum in modern diagnostic MDCT: part I. Measurement of noise power spectra and noise equivalent quanta." Phys Med Biol **52**(14): 4027-4046.

Brenner, D. J. (2010). "Slowing the increase in the population dose resulting from CT scans." Radiat Res **174**(6): 809-815.

Castaner, E., X. Gallardo, et al. (2009). "CT diagnosis of chronic pulmonary thromboembolism." Radiographics **29**(1): 31-50; discussion 50-33.

Chang, W., J. M. Lee, et al. (2013). "Assessment of a Model-Based, Iterative Reconstruction Algorithm (MBIR) Regarding Image Quality and Dose Reduction in Liver Computed Tomography." Invest Radiol.

Curry, T. S., J. E. Dowdey, et al. (1990). Christensen's physics of diagnostic radiology. Philadelphia, Lea & Febiger.

Department of Radiology, U. o. W. (2013). "CT images." from https://www.radiology.wisc.edu/COW/caseSolution.php?ref=archive&caseID=34'.

Edyvean, S. (2007). Image Noise and Low Contrast resolution - ImPACT course feb. 2007, impactscan.org.

Eldevik, K., W. Nordhoy, et al. (2010). "Relationship between sharpness and noise in CT images reconstructed with different kernels." Radiat Prot Dosimetry **139**(1-3): 430-433.

Fletcher, J. G., K. L. R. Grant, et al. (2012). "Validation of Dual-Source Single-Tube Reconstruction as a Method to Obtain Half-Dose Images to Evaluate Radiation Dose and Noise Reduction: Phantom and Human Assessment Using CT Colonography and Sinogram-Affirmed Iterative Reconstruction (SAFIRE)." J Comput Assist Tomogr **36**(5): 560-569.

Fletcher, J. G., W. R. Krueger, et al. (2013). "Pilot Study of Detection, Radiologist Confidence and Image Quality With Sinogram-Affirmed Iterative Reconstruction at Half-Routine Dose Level." J Comput Assist Tomogr **37**(2): 203-211.

Ghetti, C., O. Ortenzia, et al. (2012). "CT iterative reconstruction in image space: a phantom study." Phys Med **28**(2): 161-165.

Goodenough, D. J. and K. E. Weaver (1984). "Factors Related to Low Contrast Resolution in Ct Scanners." Computerized Radiology **8**(5): 297-308.

Grant, K., Raupach, R. (2013). "SAFIRE: Sinogram Affirmed Iterative Reconstruction." from http://usa.healthcare.siemens.com/siemens_hwem-hwem_ssxa_websites-context-root/wcm/idc/siemens_hwem-hwem_ssxa_websites-context-root/wcm/idc/groups/public/@us/@imaging/@ct/documents/download/mdaw/ndq2/~edisp/safire-00308312.pdf).

Hall, E. J. and A. J. Giaccia (2012). Radiobiology for the radiologist. Philadelphia, Wolters Kluwer Health/Lippincott Williams & Wilkins.
Heyer, C. M., P. S. Mohr, et al. (2007). "Image quality and radiation exposure at pulmonary CT angiography with 100- or 120-kVp protocol: prospective randomized study." Radiology **245**(2): 577-583.
ICRU (1996). "Medical imaging - The assessment of image quality - Int-Commiss-Radiat-Units-Measurements." Perceptual and Motor Skills **82**(3): 1391-1391.
Kalra, M. K., M. M. Maher, et al. (2003). "Low-dose CT of the abdomen: evaluation of image improvement with use of noise reduction filters pilot study." Radiology **228**(1): 251-256.
Laboratory, T. P. (2006). Catphan (R) 500 and 600 Manual. www.phantomlab.com.
Ludewig, E., A. Richter, et al. (2010). "Diagnostic imaging--evaluating image quality using visual grading characteristic (VGC) analysis." Vet Res Commun **34**(5): 473-479.
Martinsen, A. C. T., H. K. Saether, et al. (2012). "Iterative reconstruction reduces abdominal CT dose." Eur J Radiol **81**(7): 1483-1487.
McNitt-Gray, M. F. (2002). "AAPM/RSNA physics tutorial for residents: Topics in CT - Radiation dose in CT1." Radiographics **22**(6): 1541-1553.
Merran, S. and A. K. Dixon (1991). CT & MRI radiological anatomy. Oxford ; Boston, Butterworth-Heinemann.
Nishikawa, R. M. (2013). "The fundamentals of MTF, Wiener Spectra and DQE." from https://www.aapm.org/meetings/99AM/pdf/2798-87374.pdf.
NRPA (2010). Radiologiske undersøkelser i Norge per 2008, Norwegian Radiation Protection Authority.
NRPA (2013). Regulation on radiation protection.
Romans, L. (2013). "CT Image Quality." from http://www.cewebsource.com/coursePDFs/CTimageQuality.pdf.
RSNA.org. (2013). from http://www.rsna.org/uploadedFiles/RSNA/Content/Science_and_Education/Quality/Mehta.pdf.
Siemens. (2007). "Somaton Definition Application Guide." from http://www.medical.siemens.com/siemens/en_GB/gg_ct_FBAs/files/CIP/appl_guides/ApplicationsGuide_Definition.pdf.
Siemens. (2013). "Care Dose 4D." from http://www.medical.siemens.com/siemens/de_DE/rg_marcom_FBAs/files/news/CT_Dose_Reduction/DoseReduction_Sessions_19_RSNA_DRUCK.pdf.
Singh, S., M. K. Kalra, et al. (2012). "Comparison of hybrid and pure iterative reconstruction techniques with conventional filtered back projection: dose reduction potential in the abdomen." J Comput Assist Tomogr **36**(3): 347-353.
Singh, S., M. K. Kalra, et al. (2010). "Abdominal CT: Comparison of Adaptive Statistical Iterative and Filtered Back Projection Reconstruction Techniques." Radiology **257**(2): 373-383.
Smith, A. (2009). "PSFs in IDL." from http://www.anthonysmith.me.uk/research/2009/03/18/psfs-in-idl/.
Smith, S. W. (2002). The Scientist and Engineer's Guide to Digital Signal Processing.
Sprawls, P. (1992). "AAPM tutorial. CT image detail and noise." Radiographics **12**(5): 1041-1046.

von Falck, C., V. Bratanova, et al. (2013). "Influence of sinogram affirmed iterative reconstruction of CT data on image noise characteristics and low-contrast detectability: an objective approach." PLoS One **8**(2): e56875.

Wang, R., U. J. Schoepf, et al. (2013). "CT coronary angiography: image quality with sinogram-affirmed iterative reconstruction compared with filtered back-projection." Clin Radiol **68**(3): 272-278.

Webb, S. (1988). The Physics of medical imaging. Bristol ; Philadelphia, Hilger.

Webb, S. and M. A. Flower (2012). Webb's physics of medical imaging. Boca Raton, Taylor & Francis.

Weston, J. (2007) "Principles of CT scanning."

Winklehner, A., C. Karlo, et al. (2011). "Raw data-based iterative reconstruction in body CTA: evaluation of radiation dose saving potential." Eur Radiol **21**(12): 2521-2526.

www.radiologie-idar-oberstein.com. (2013). from http://www.radiologie-idar-oberstein.com/html/computertomographie1.html.

Yang, W. J., F. H. Yan, et al. (2013). "Can Sinogram-Affirmed Iterative (SAFIRE) Reconstruction Improve Imaging Quality on Low-Dose Lung CT Screening Compared With Traditional Filtered Back Projection (FBP) Reconstruction?" J Comput Assist Tomogr **37**(2): 301-305.

Yang, W. J., F. H. Yan, et al. (2013). "Can Sinogram-Affirmed Iterative (SAFIRE) Reconstruction Improve Imaging Quality on Low-Dose Lung CT Screening Compared With Traditional Filtered Back Projection (FBP) Reconstruction?" J Comput Assist Tomogr **37**(2): 301-305.